MER 85-86 LOD-PJW1

EFFECTS OF NITROGEN ION IMPLANTATION ON THE BEHAVIOR OF STEELS IN SLIDING CONTACT

PREPARED FOR

THE ADOLPH COORS COMPANY

GOLDEN, COLORADO

by

Larry O. Daniels

Approved by

Paul J. Wilbur

November 1985

Department of Mechanical Engineering
Colorado State University
Fort Collins, Colorado

ABSTRACT

Effects of Nitrogen Ion Implantation on the

Behavior of Steels in Sliding Contact

Nitrogen ion implantation and its effects on AISI M2 tool steel, SAE 01 tool steel and AISI type-304 stainless steel are discussed. To implant the steels, a relatively new ion implantation system was used that is able to deliver high ion beam current densities (>1500 $\mu A/cm^2$) and operate for extended periods of time at implantation energies of 20-80 keV on a variety of gases. It is shown from Auger electron spectroscopic analysis that nitrogen concentrations in the near-surface layers of the steels in this study can reach 30 atom % by using a 60 keV nitrogen ion beam. Nitrogen-implanted AISI M2 tool steel is shown to exhibit a 27% reduction in wear in comparison to unimplanted M2 tool steel after over 5 km of lubricated sliding-contact wear. SAE 01 tool steel is shown to exhibit a 63% reduction in wear under similar wear conditions. These results are demonstrated on tool steels treated with 60 keV nitrogen ions to an implanted ion dose of 2×10^{17} N_2^+/cm^2 at an ion beam current density of 100 $\mu A/cm^2$. For nitrogen-implanted AISI type-304 stainless steel the load-bearing capacity is shown to increase to a level over 40 times that of unimplanted 304 stainless steel. The load-bearing capacity is found to be a function of the nitrogen ion dose and the ion beam energy. Finally, nitrogen concentration profiles and implantation surface temperatures of AISI type-304 stainless steel samples that have been implanted with ion beam current densities of 10 $\mu A/cm^2$, 100 $\mu A/cm^2$ and 1500 $\mu A/cm^2$ are compared. The data indicate that nitrogen diffusion inward from the surface occurs in AISI type-304 stainless steel during implantation at an ion beam current density that is sufficiently high (1500 $\mu A/cm^2$) to cause surface temperatures to rise to ~450°C.

TABLE OF CONTENTS

TABLE OF CONTENTS (cont'd)

LIST OF FIGURES

LIST OF FIGURES (cont'd)

LIST OF TABLES

I. INTRODUCTION

Wear of steel surfaces on components such as extrusion dies, bearings, and a multitude of other machine components, results in large costs to industry. Currently, some of the solutions used to reduce the problem of wear are i) lubrication of contacting components, ii) fabrication of the components from wear resistant and usually expensive materials, iii) application of wear resistant coatings and iv) application of case hardening. Case hardening is used to increase the nitrogen or carbon content by heating the component and allowing nitrogen or carbon to diffuse into the surface.

By using an alternative surface modification technique called ion implantation, one can increase the wear resistance of a material and yet maintain properties such as toughness in the bulk of the material. In fact, over an order of magnitude decrease in the wear rate of nitrogen-implanted steels compared to unimplanted steels has been reported.[1] This surface modification technique is a process whereby any element that can be ionized may be deposited into the near-surface layers of any solid material. Ion implantation is accomplished by creating positively charged ions, accelerating them to high energies through an electric field and allowing them to strike a solid surface.

Ion implantation affects a layer of the target surface that is only a few hundred nanometers thick. The effects are caused by ions losing their energy predominantly by elastic nuclear collisions[2] and as a

result displacing target atoms. In this way, an amorphous solid is usually obtained in the near-surface layers of the target, even though the target material may have had a crystalline structure before the ion implantation process was accomplished. The new amorphous surface layer consists of a chemical combination of implanted ions* and target atoms and/or a simple solid mixture of the two materials. Although the concentration of implanted atoms may be very high in the amorphous surface, it is typically limited to 50 atom%[3] due to a process accompanying implantation called sputtering. Sputtering is a phenomenon in which atoms are removed from the target surface due to collisional processes. An equilibrium point is reached when the number of previously implanted atoms being sputtered from the target surface is equal to the number of atoms being added to the surface by implantation.

Ion implantation has several advantages over the other common material surface modification processes such as the application of coatings or case hardening. Some relative advantages of ion implantation are:

1. No adhesion problems exist. The ions penetrate the target surface to different depths that are determined by the implantation energy and the materials involved. As a result, no distinct interface exists between the implanted surface layers and the bulk target materials. In contrast to implanted surfaces, coated surfaces contain a clear interface between the coating and the substrate. Quite

---

*The implanted ions become neutral particles by combining with the free electrons in the target material immediately after coming to rest.

often, adhesion problems develop at this sharp interface.

2. The average ion penetration depth is controllable. Two implantation parameters are used to control the ion penetration depth. First, when the ion energy is increased, the ions penetrate the surface to a greater average depth. Second, by allowing the target temperature to increase during implantation, the implanted-atom diffusion coefficient increases[4], and the implanted ions are able to diffuse to greater depths.

3. Nonequilibrium surface layers are possible. In conventional alloying processes, a solid solubility limit is reached and the addition of more of an alloying element results in precipitation of the element. The concentration of the alloying element reaches a maximum and cannot be increased. By using ion implantation, one can for example achieve implanted-nitrogen atom concentrations in stainless steel that are over 40 atom%.[5] This exceeds the solid equilibrium solubility limit.[4]

4. No significant dimensional changes occur in the implanted component. Components that have gone through their final finishing process, may be implanted and be ready for use. With coating processes or case hardening, the component must either be machined to correct dimensions after the process or be designed such that its dimensions are correct after the process is completed. In addition, warping of the component sometimes occurs because of the high temperatures necessary to perform case hardening.

5. Accurate control of the amount of implanted material is readily accomplished. One simply regulates the rate at which the ions strike the target surface (by controlling the ion beam current) and the time that the surface is being implanted to control the implanted-atom concentration. In case hardening, it is sometimes difficult to control the nitrogen or carbon concentration, because the diffusion rates vary due to variations in temperature, surface geometry, and surface barriers such as oxide films.
6. New alloys can be formed using ion implantation. Many materials cannot be combined by using conventional methods because their melting temperatures are very different. By using ion implantation, a solid mixture of any combination of ionizable elements and a solid may be formed.
7. A small quantity of implanted material is required. Because only a few hundred nanometers of near-surface layers are affected by implantation, very little implanted material is used to effect changes in the wear resistance. This is important when one is using expensive materials.

As with all processes, ion implantation has certain limitations. These limitations are:

1. In-vacuum processing is required. This increases the processing cost and the difficulty associated with manipulation and temperature control of the target.
2. Ion implantation is a line-of-sight process. Any target surface that cannot be exposed directly to the ion beam cannot be implanted.

3. Only shallow target penetration is possible. Usually, less than 1 μm of the target surface is affected by ion implantation. This causes the process to be less attractive to industries such as mining, where erosive wear of surfaces is large.
4. Ion implantation technology is relatively new. Because it is new, many areas of ion implantation still need to be studied. In addition, implantation equipment is not yet readily available at low prices.

History

Effects of Nitrogen Implantation on Steels

Although ion implantation has been used to improve material properties such as corrosion and fatigue resistance of various alloys,[1,6,7] the majority of work accomplished has involved the use of nitrogen implantation into various steels to improve wear resistance. Many steels have shown increased wear resistance after being case-hardened with nitrogen.[8] Therefore, nitrogen implantation of steels was a logical initial research topic to determine if it had the same effect on steels as case hardening does.

The types of steels on which nitrogen ion implantation research has been conducted were put into three general categories for this thesis. They are i) hard, low-chromium steels with Rockwell C hardness greater than 55 and chromium concentration of less than 5 atom%, ii)

soft, low-chromium steels with Rockwell C hardness less than 55 and iii) austenitic stainless steels.

Conflicting reports exist as to whether or not an improvement in wear resistance of hard, low-chromium steels is obtained by using nitrogen ion implantation. Several researchers have reported that nitrogen implantation does not improve the wear behavior of hard bearing steels such as AISI 52100.[9-12] However, Hirvonen[7] reported that a factor-of-two improvement in wear resistance was commonly found for nitrogen-implanted AISI 52100 steel samples. To assess the wear behavior of very hard steels which have been implanted with nitrogen, AISI M2 tool steel (Rockwell C hardness, 58-62) was used in the present study. No specific literature was found on nitrogen ion implantation of AISI M2 tool steel.

Soft, low-chromium steels have exhibited improvement in wear resistance through the use of nitrogen ion implantation.[6,7,10,13-16] For example, Dimigen et al[10] reported a 70% reduction in the wear rate of nitrogen-implanted AISI 4140 steel in comparison to unimplanted 4140 steel. The soft, low-chromium steel that was implanted with nitrogen and wear tested in the present study was SAE O1 tool steel. Again, no published literature was found pertaining to nitrogen ion implantation of this specific steel.

Generally, stainless steels implanted with nitrogen have shown the greatest amount of improvement in wear resistance.[1,5,7,10,12-14] Most researchers have reported at least an order of magnitude of improvement in wear resistance of stainless steels with nitrogen implantation. In addition to improving wear resistance, Hirvonen[1] reported that nitrogen implantation appeared to improve the load-bearing capacity of a system

consisting of AISI type-416 stainless steel. The present study involves quantitative testing of the load-bearing capacity of unimplanted and nitrogen-implanted type-304 stainless steel.

To study the wear of ion-implanted components, several varieties of wear tests have been used. The majority of wear tests have involved a stationary or oscillating steel pin or ball being forced against a flat, rotating steel disc in a direction normal to the disc surface to obtain sliding-contact wear.[1,10,11] In the present study, a Fayville-LeVally Wear and Friction Test Machine was used that also provided sliding-contact wear. But the wear in this case occurred between a stationary steel block and a rotating steel ring. No literature was found in which block was forced against a rotating ring to study tribological effects of ion implantation.

In addition to wear testing, implanted-material surfaces have been studied by several surface analysis techniques.[5,10,11,14,17,18] One technique which has been frequently utilized is Auger electron spectroscopy (AES) used in conjunction with ion sputtering.[9,11,13] Implanted-ion concentrations have been obtained through AES by sputtering material surface layers away with an ion gun, then impacting the surface with electrons and examining the recoiling Auger electrons. To determine the implanted-nitrogen concentration profiles of the rings and blocks in the present study this procedure of sputtering away surface layers with argon ions in conjunction with AES was used.

Implantation Equipment

In addition to wear testing of implanted materials, an important area of discussion concerns the equipment that has been used to ion-implant these materials. Originally, ion implantation equipment was developed to add small concentrations of impurities to specified depths in semiconductor materials in order to obtain desired electrical properties. In the early 1970's, it was discovered that in addition to electrical properties, tribological, chemical and optical properties could be affected through the use of ion implantation. Even though the available implantation equipment at that time was designed for use on semiconductor materials, its use on non-semiconductor materials resulted in significant (and usually improved) changes in surface properties. Up to this point, the majority of implantation work on non-semiconductor materials has been accomplished with implantation systems designed for semiconductor applications.

In Fig. 1, a schematic of a typical ion implantation system developed for semiconductor applications is shown.[19] To implant a semiconductor material with the system in the figure, a chemical element containing the atom to be implanted is first fed into the ion source at low pressure. The atoms are then ionized and extracted electrostatically from the ion source into a high vacuum environment by the extraction electrode to form a moderately energetic ion beam (10-30 keV). The ions are then collimated into a thin ion beam by the first analyzer slit and separated according to ion mass by the analyzer magnet. In this example, three different ions (A, B and C) are affected by the magnet's magnetic field so that the medium mass ions (B) are passed through the second analyzer slit. From the second analyzer slit,

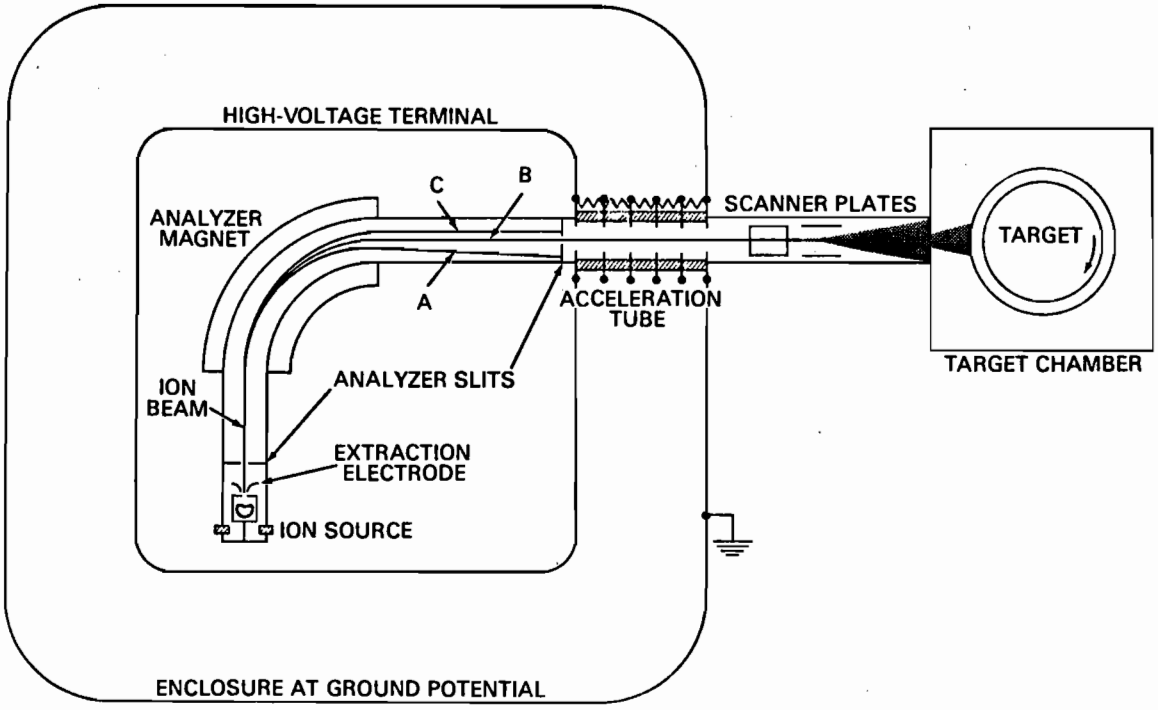

Figure 1. Ion Implantation System Designed for Semiconductor Implantation (from Butler, 1980)

the selected ions are accelerated to implantation energies (35-100 keV) by the acceleration tube and rastered by the scanner plates over a selected area. Finally, the rastered beam is partially blocked, and this results in a selected implanted area on the target (which in this example is shown rotating to allow all around implantation and power dissipation).

In contrast to the ion implantation systems designed for semiconductor applications, the Colorado State University (CSU) system used in the present study was designed from electric propulsion principles and had been developed specifically to affect surface properties of non-semiconductor materials. Hereafter for convenience, the implantation systems designed for semiconductor applications will be referred to as the "previous systems" and the CSU implantation system designed and used for non-semiconductor applications in the present study will be called the "CSU system". The main ion beam parameters in the CSU system[20] that are different from parameters in the previous implantation systems are:

1. Ion beam current density. Ion beam current density is equal to the rate at which ions strike a target surface, therefore a higher current density results in a larger ion dose (number of implanted ions per unit area) within a given implantation time. Previous systems, in general delivered low ion beam current densities (10 $\mu A/cm^2$)[21-25] compared to the CSU system that can deliver well over 1500 $\mu A/cm^2$. The previous low ion beam current density implantation systems were adequate because relatively low ion doses (10^{11}-10^{16} ions/cm^2)[26] were implanted into semiconductor materials.

Because significantly higher ion doses (10^{16}-10^{18} ions/cm^2) were necessary to affect non-electrical properties of materials,[3] much longer implantation times (on the order of hours) were required when the previous systems were used. The CSU system is capable of implanting large ion doses in a matter of minutes due to its high ion beam current density capability.

2. Ion beam purity. To obtain specific electrical properties in semiconductor materials with ion implantation, very high ion beam purity was necessary, resulting in complicated implantation systems with the analyzer magnet shown in Fig. 1. Because the ion beam purity is not as important when affecting tribological properties, mass analysis of the ion beam is not used in the CSU system. This allowed the CSU system to be made much simpler and more efficient than previous implantation systems.

3. Ion beam diameter. Because the portion of the ion beam which had a relatively uniform current density in the CSU system was large (about 3 cm diameter), rastering of the beam was not required. This eliminated the need for scanner plates because the beam was broad enough to effectively implant a large target area. In contrast, beam diameters of previous systems were relatively small (0.4 cm to 1.0 cm).[3]

II. EXPERIMENTAL APPARATUS AND PROCEDURE

Overview

For this work, a comparative study of the differences in wear behavior of unimplanted and nitrogen-implanted steels was performed in the following manner. First, the surfaces of the steel samples were modified from "as received" finishes to more uniform finishes. Then, after very thoroughly cleaning the samples, selected ones were nitrogen-implanted with the broad beam, high current density implanter. To measure the nitrogen concentration of representative implanted samples, Auger electron spectroscopy was used. The next step, which was the major focus of this research, was to wear test all of the implanted and unimplanted samples on a Fayville-LeVally Wear and Friction Test Machine. The wear of implanted steel was measured and compared to the wear of unimplanted steel. Finally, qualitative comparisons of the surface morphology of worn and unworn areas on selected implanted and unimplanted steel samples were made using a scanning electron microscope.

Test Sample Description and Preparation

The steel test samples used in the present study consisted of the steels having the hardnesses and compositions shown in Table 1.

Table 1

Composition and Hardness of Steels

Classification	Designation	Hardness (Rockwell C)	Composition (weight%)
Tool steel	AISI M2	58-62	0.85%C, 4%Cr, 5%Mo, 6%W, 2%V
Tool steel	SAE O1	27-33	0.9%C, 1.2%Mn, 0.5%W, 0.2%V 0.5% Cr *
Stainless steel	AISI type-304	17-21	0.08%C, 19%Cr, 9%Ni

The hardnesses were obtained from the steel sample manufacturer and the compositions of the samples were found in Ref. 27. Because a Fayville-LeVally Wear and Friction Test Machine was used, the necessary sample configuration for each wear test consisted of a block that was subjected to lubricated sliding-contact against a ring. The blocks were 1.6 cm by 0.6 cm by 1.0 cm and the 1.6 cm by 0.6 cm region on the blocks was implanted and wear tested. The outside diameter of the rings was 3.5 cm. The standard blocks and rings which were used are described further in ASTM Standard D2714(1978).

The steel ring and block samples were obtained from the Falex Corporation with a wide range of surface finishes. To be certain that the changes in wear resistance were caused by nitrogen implantation, it was necessary to obtain more uniform surface finishes. For the SAE O1 tool steel samples and the AISI type-304 stainless steel samples, the important surfaces that were to be implanted and later wear-tested, were polished with a fine buffing compound having about the same particle size as rouge. The samples were changed from "as received" finishes of 0.15-0.30 μm rms to modified finishes of 0.10-0.15 μm rms. Because

*Ref. 27 gives 0.9% C, 0.5% Cr, 0.5% W does not give Mn or V

the "as received" surface finishes of the AISI M2 tool steel rings were much rougher (0.55-0.68 μm rms) than the other samples, the M2 rings were first ground with about a 150 grit grinding wheel, then sanded and finally buffed to obtain modified finishes of 0.10-0.15 μm rms. Selected ring finishes were measured with a profilometer after being modified. The M2 tool steel blocks were received with surface finishes of 0.30-0.15 μm rms and as a result they were simply buffed to obtain the 0.10-0.15 μm rms finish.

Just prior to implantation, the rings and blocks were cleaned ultrasonically in chlorathene for several minutes and then rinsed off with acetone. After cleaning, the samples were handled only with lint-free tissue before they were implanted.

Implantation

The ring and block samples (targets) were implanted using the CSU implantation system that was designed and constructed specifically to implant non-semiconductor materials. A schematic representing the implantation system used in the present study is shown in Fig. 2. The major components of the system were an ion source, a mask to block a portion or all of the ion beam, and a fixture to support the implantation targets downstream of the ion source. All of the above components were enclosed in a 0.4 m diameter by 1.2 m long vacuum chamber that operated at a pressure in the high 10^{-6} torr range during operation of the implanter.

To implant targets, such as the rings and blocks with the system shown in Fig. 2, atoms were first fed from the neutral gas bottle into

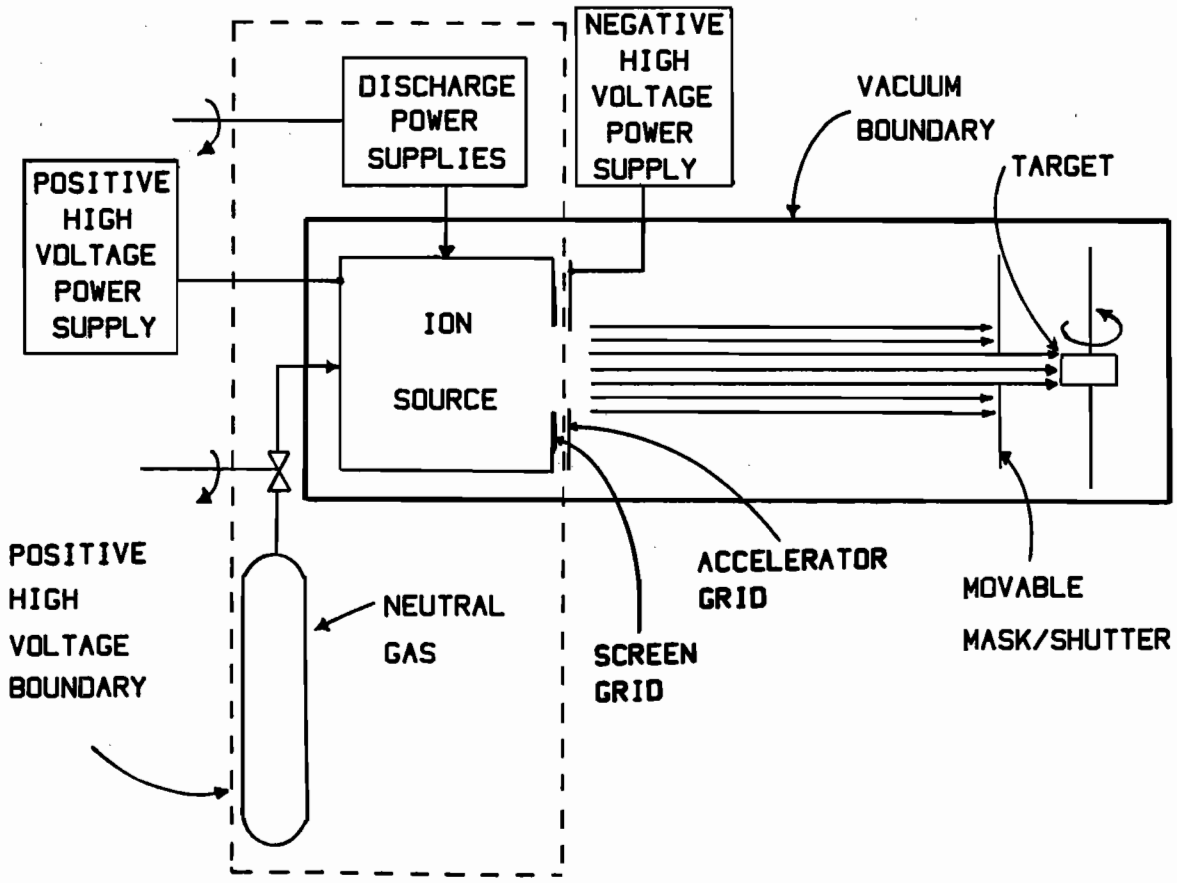

Figure 2. Schematic of the CSU Ion Implantation System Used in this Study

the cylindrical ion source (at positive high voltage relative to ground). While in the ion source, the atoms were ionized through electron bombardment[28] which was enabled by the discharge power supplies. The resulting positive ions were extracted and focused into a broad, collimated beam from the ion source by the potential difference created between the screen grid at ion source potential and the accelerator grid at negative high voltage. The two grids shown in Fig. 2, consisted of circular stainless steel plates with one aperture in the center of each plate through which the ion beam passed. During this study, ion beams were created with currents and energies up to 50 mA and 80 keV, respectively. The ions in the beam were directed downstream toward a movable mask/shutter system that was used to interrupt all or a portion of the ion beam before it reached the target material. The mask/shutter system was constructed of graphite sheets* mounted on the upstream side of a copper plate. After the ion source had stabilized, the mask/shutter system was positioned so the beam ions would strike the target at the proper location. The target (block or ring) was located about 50 cm downstream from the accelerator grid. The implantation targets were supported by a fixture that allowed one sample after another to be transported into the ion beam. The fixture also had the capability of rotating the targets in the direction shown in Fig. 2 while they were being implanted. The rotation capability allowed the rings to be implanted over their entire outside diametrical surfaces.

---

*The graphite was used because it was able to withstand the high temperatures that sometimes occurred during operation of the implanter.

In addition to the fixture providing support for the samples (targets), it along with the mask/shutter system helped to keep the samples cool during implantation. It was necessary to keep the targets cool during implantation because ions impart their energy to target atoms, and as a result the target temperature increases. The target can become sufficiently hot to cause the implanted nitrogen to diffuse outward from the surface and reduce the effects of ion implantation. Flow of water through the interior of the fixture provided the necessary target cooling by conducting away the heat. The heat generated from the energy of the ions, flowed from the targets through a copper support(s) (the copper supports used for the rings were different in shape in comparison to the support used for the blocks) and eventually to the cooling water. On the other hand, the mask/shutter system helped to keep the samples cool by interrupting the portion of the ion beam that would have heated the fixture and therefore have increased the thermal load on the cooling system. Temperature measurements of the surfaces of selected blocks during nitrogen implantation were taken, to learn if the cooling mechanisms just described were adequate. These data appear in Appendix A.

In order to calculate the dose of ions implanted into a target, it was necessary to know the ion beam current density at the target. During operation of the implantation system, the ion beam current density was measured by rapidly sweeping a probe along an arc passing through the beam centerline at a location 50 cm downstream of the accelerator grid. The probe consisted of a small disc of known area through which a portion of the ion beam current passed and was measured. A more detailed description of the probe is given in Ref. 29 In Fig. 3,

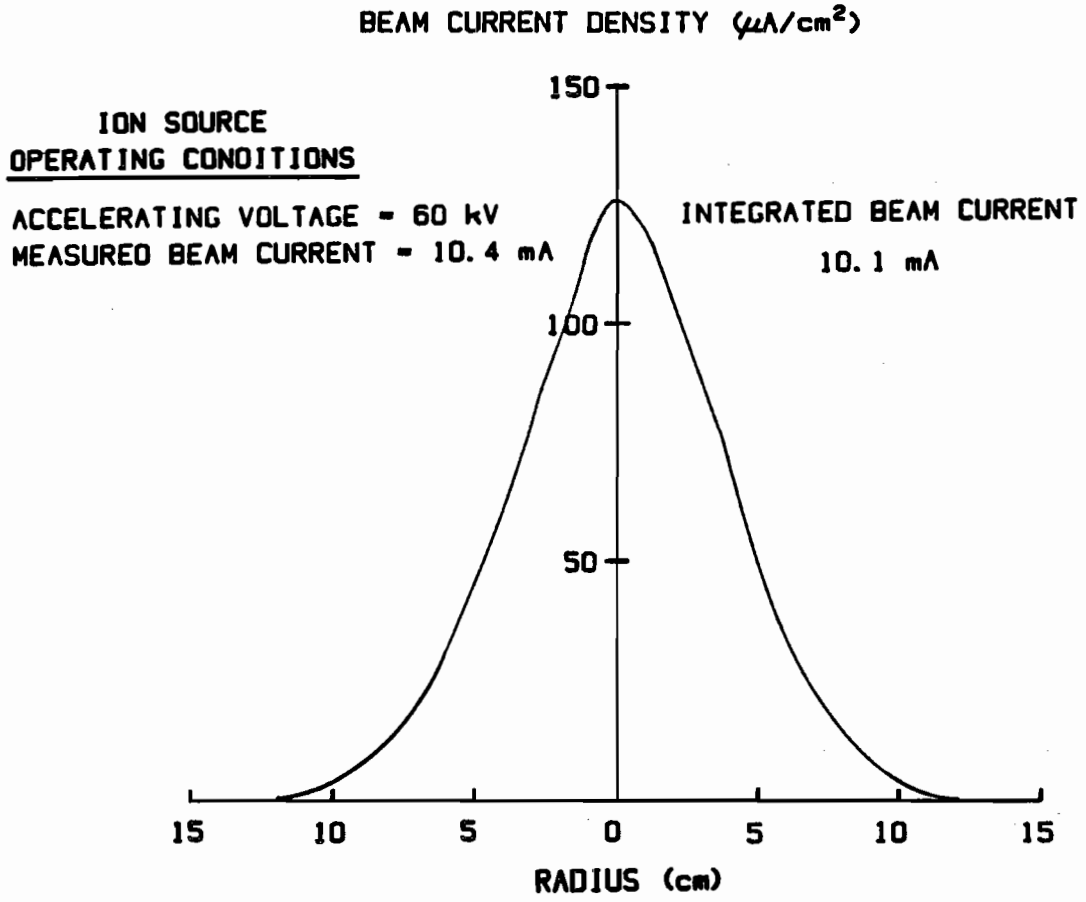

Figure 3. Nitrogen Ion Beam Current Density Profile

a typical plot of ion beam current density as a function of ion beam radius is shown. For this example, the ion accelerating voltage was 60 kV and the measured ion beam current was 10.4 mA. These operating conditions produced a peak current density of 125 $\mu A/cm^2$ and an ion beam diameter of 25 cm. To be certain the probe was operating properly, the integrated beam current, J_B(mA) was found from the following equation:

$$J_B = \pi \int_{-r_T}^{r_T} j_B(r) r dr \qquad (1)$$

where r_T(cm) is the total ion beam radius at the probe location (50 cm downstream from the accelerator grid), and $j_B(r)(mA/cm^2)$ is the ion beam current density at the radius r(cm), measured from the ion beam centerline. The integrated ion beam current was then compared to the measured ion beam current. In the example shown in Fig. 3, the integrated ion beam current was 2.9% less than the measured ion beam current. For all of the beam current density profiles, the integrated ion beam currents were within 10% of the measured ion beam currents over the total range of operating conditions for the ion source.

To implant the rings and blocks, the initial part of the procedure was the same for each type of target. First, the ion source was started and set to preselected operating conditions. This was done while the samples which were mounted on the fixture were being maintained at the cooling water temperature (10-15 ^{o}C). The samples were shielded from the ion beam by the mask/shutter system until the ion source reached steady state operating conditions. At this point, the implantation procedure for the rings was somewhat different from the one for the blocks.

To implant the rings, the shutter was removed and one or two rotating ring surfaces were exposed to the ion beam after it had passed through a mask having aperture dimensions of 1.0 cm by 2.0 cm (one ring) or 2.0 cm by 2.0 cm (two rings). The portion of the ion beam passing through the mask was allowed to strike the ring(s) for a period of time which yielded the desired implanted-nitrogen ion dose. Because the rings had to be rotated by the fixture during implantation, the water could not be circulated through the fixture. For this reason, if the fixture portion which extended outside of the vacuum chamber felt hot (~100 ^{o}C) during implantation, the ion beam was interrupted with the shutter and water was circulated through the fixture to cool the target ring(s). After the ring(s) was cool (~15 ^{o}C), the shutter was removed to again allow the ion beam to strike the rotating ring(s) until the total required implantation time was reached. The shutter was then moved into place to completely interrupt the ion beam, the next ring(s) to be implanted was moved into place and the procedure was repeated until all of the rings which were mounted on the copper supports, had been implanted.

Because the blocks did not have to be rotated while they were being implanted, it was possible to cool them continuously with circulating water. When the ion source was operating stably, the shutter was moved to allow the ion beam to pass through a selected mask with aperture dimensions of 1.7 cm by 0.7 cm or 1.7 cm by 1.5 cm depending on whether one or two blocks were being implanted. The ion beam was then allowed to strike the block(s) immediately downstream of the mask/shutter system. After the block(s) had been exposed to the ion beam for the period of time which yielded a desired ion dose, the shutter was moved

to interrupt the ion beam. As was done with the rings, the fixture was then moved into the correct location to implant another block(s) and the procedure was repeated until all of the blocks mounted in the copper support structure had been implanted.

The specific implantation parameters used for both of the tool steels studied, were the same. They were implanted with 60 keV nitrogen ions to a dose of 2×10^{17} N_2^+/cm^2 and at a current density of 100 $\mu A/cm^2$. For each test, both the ring and the block to be worn against each other were implanted to these same conditions.

Three groups of tests were conducted on the AISI type-304 stainless steel samples. Similar to the tool steel samples, all ring/block test couples were implanted to equal conditions. The groups of samples were implanted for the indicated reasons at each of the following implantation conditions:

1. To determine the dose which would result in the highest load-bearing capacity (galling load) between ring and block surfaces, several rings and blocks were implanted with 60 keV nitrogen ions at current densities of 100 $\mu A/cm^2$, 300 $\mu A/cm^2$ and 1500 $\mu A/cm^2$ and various doses ranging from 5×10^{15} to 1×10^{18} N_2^+/cm^2.
2. To determine the ion energy which would result in the highest load-bearing capacity (galling load) between ring and block surfaces at a selected current density of 300 $\mu A/cm^2$ and a dose of 5×10^{16} N_2^+/cm^2, the implanted-ion energy was varied from 35 to 80 keV.
3. To study the effect of nitrogen diffusion during implantation, three blocks were implanted with 60 keV

nitrogen ions to a dose of $1x10^{17}$ N_2^+/cm^2 and current densities of 100 $\mu A/cm^2$, 300 $\mu A/cm^2$ and 1500 $\mu A/cm^2$. The surface temperatures of blocks implanted at these current densities were recorded during the implantation process using iron-constantan thermocouples. These thermocouples were soldered to the bottom of a hole which was within 0.1 mm of the surface being implanted. Upon completion of the implantation process and the recording of the block surface temperature history during implantation, Auger electron spectroscopic analysis was performed on each sample to determine the nitrogen concentration at various depths into the block surfaces.

Auger Electron Spectroscopic Analysis

Auger electron spectroscopic (AES) depth profiling of selected nitrogen-implanted rings and blocks was accomplished in an ultra high vacuum facility ($2x10^{-7}$ torr, working pressure) with a Physical Electronics Industries (PHI) Model-548 system. The portion of the system that was used in this study, consisted of an electron gun, an x-ray source, an energy analyzer and an argon ion gun.

To perform the Auger analysis on a selected implanted ring, a 1.3 cm long section was cut from the ring with a water-cooled abrasive saw and the ring section was placed in the PHI vacuum chamber. After the vacuum system was pumped to a pressure in the low 10^{-8} torr range, a 5 kV argon ion gun which delivered an ion beam current density of 140 $\mu A/cm^2$ was directed over a 0.05 cm^2 area on the ring section surface for

2 minutes to remove a thin material layer.* Next, the electron gun was directed at the ring section and the Auger electrons produced at the surface by the incident electron beam were analyzed with the energy analyzer to find the relative amounts of nitrogen and iron at that depth. Then the ion gun was again directed at the surface to remove more material and the procedure was repeated until the ion-sputtered crater was sufficiently deep so that very little nitrogen could be detected. The reader is referred to Appendix C for the nitrogen concentration determination from the Auger data. Sensitivity values, which are a measure of the number of Auger electrons that are emitted per incident electron for a specific material were found in Ref. 30 for iron, nitrogen and carbon. X-ray photoelectron spectroscopy (XPS)[31] was also performed on selected samples to verify the results obtained from AES. The blocks were analyzed, in the same manner as the rings.

Because the rate (nm/sec) at which the argon ion gun sputtered away material from the sample surfaces was not known, it was necessary to determine this rate for each of the sample materials. This was accomplished by requiring the implanted-nitrogen ion dose (as determined by the product of ion current density and implantation time) to be equal to the dose determined by finding the area under a plot of nitrogen atom density vs. sputtering time. The details of the method are given in Appendix B.

---

*The thickness of the removed layer for 2 minutes of sputtering time was found to be about 5.0 nm for AISI type-304 stainless steel as given in Appendix B.

Wear Testing

To wear test the rings against the blocks, an Alpha Model LFW-1 Wear and Friction Test Machine, manufactured by the Fayville-LeVally Corporation, was used. The schematic in Fig. 4 illustrates the principle on which this friction and wear test operated. For each test, a block was held in the test machine and forced in a normal direction against a ring that was mounted on a rotating shaft. The normal force that was applied between the block and the rotating ring could be varied from 44 N(10 lb_f) to 3560 N(800 lb_f) in 44 N increments and the shaft rotation speed could be varied from 10 to 800 rpm. The friction force that was created between the sliding ring and block surfaces, was sensed by the load cell shown in Fig. 4 and recorded by a strip chart recorder. The test apparatus also included a lubricant reservoir, containing gear oil 150 that partially submerged the rotating ring. The wear procedure used for the tool steels was different from the procedure used for the stainless steel. Each procedure is described in the following paragraphs.

Conventional Wear Testing

The tool steels (AISI M2 and SAE 01) were wear tested by first mounting a ring and block (both of which had received the same surface treatment) into the wear test machine in the configuration shown in Fig. 4. The lubricant reservoir was then filled with gear oil 150 (kinematic viscosity = 1.50 cm^2/sec at 40 ^oC) to submerge approximately half of the ring and the load to be applied between the ring and block surfaces was

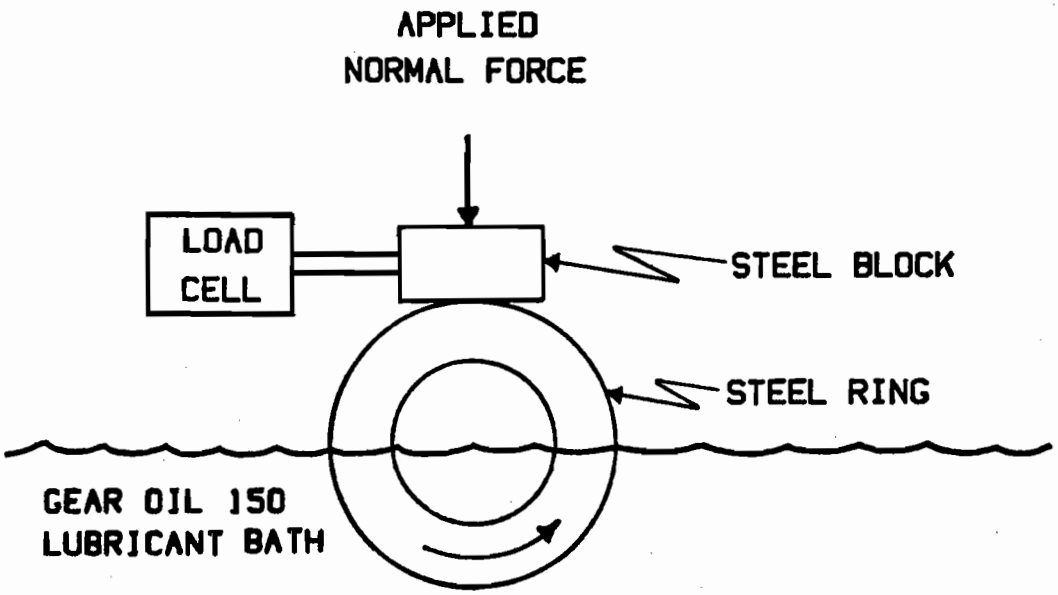

Figure 4. Wear and Friction Test Configuration

selected. Next, the ring was rotated at 190 rpm (corresponding to a sliding velocity between the ring and block surfaces of about 35 cm/sec). After the ring rotational velocity was stable at 190 rpm, the load between the stationary block and rotating ring surfaces was ramped up linearly in about five seconds so overload effects due to uneven or rapid loading could be avoided. At the same time that the load was being applied, the strip recorder that was used to record the friction force, was turned on and the 30 minute wear test time was started. Upon completion of the 30 minute interval, the wear test machine stopped the ring rotation and the test block was removed from the wear test apparatus. The length L(mm), of the wear scar that formed on the test block shown in Fig. 5, was measured in three places (two measurements near each block edge and one in the center). This was done with a Finescale comparator that consisted of a magnifying lens and a scale with an accuracy of $\pm$0.05 mm. This accuracy corresponded to errors in the wear scar measurements of generally less than 5%. The wear scar measurements were then averaged and the volume of material removed from the block was calculated. The specific equations used to calculate this value are given in Appendix D. Upon completion of the wear scar measurements the block was reloaded against the ring in the wear test machine and wear tested for another 30 minute interval. This was repeated until a total sliding distance of over 5 km had been achieved.

The SAE O1 tool steel was wear tested at a lower load than the AISI M2 tool steel but the test procedures were in all other respects the same. The lower normal load was applied to the SAE O1 samples because testing these samples at the higher load caused severe wear and galling of these ring and block surfaces. This in turn caused the friction

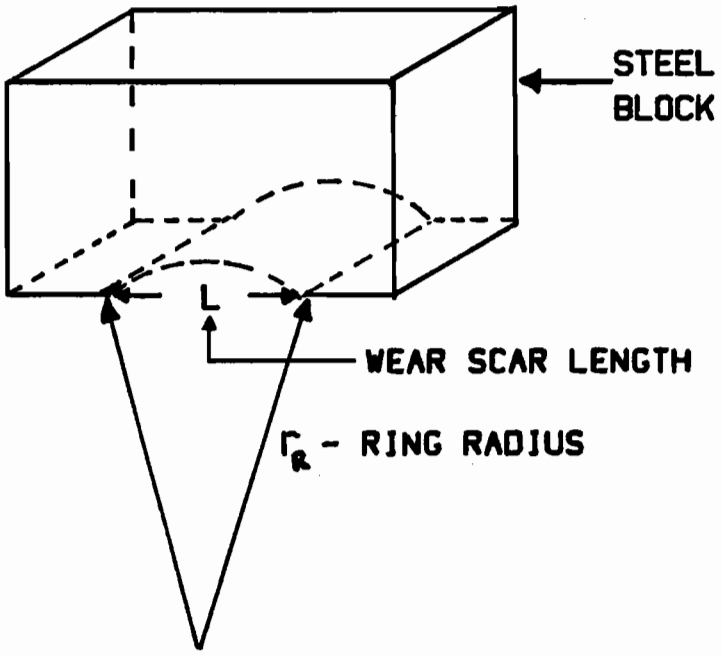

Figure 5. Schematic of Steel Block with Wear Scar

force to exceed the test machine limit. Normal loads of 2225 N and 2670 N were applied between the SAE O1 and AISI M2 tool steel surfaces, respectively.

Galling Failure Testing

A different testing procedure than the one used for the tool steel samples was used for the AISI type-304 stainless steel samples because small normal loads between the unimplanted stainless steel ring and block surfaces (i.e., loads less than 100 N) caused severe adhesive wear (galling) between the two surfaces. This type of wear prevented accurate wear scar measurements on the blocks because: i) during a test, much ring material was transferred to the block ii) the wear scar was very non-uniform and iii) when the severe wear began, the test had to be stopped within ~2 seconds to prevent damage to the wear test machine due to the high friction forces that developed. Therefore, a test was developed to measure the normal load at which severe adhesive wear (galling) occurred. This test is similar to the one described in ASTM Standard D2782(1977) to determine score values of different lubricants.

The different test procedure used for the AISI type-304 stainless steel samples will be called the galling load test, hereafter. This test was conducted by installing a test ring and block in the Fayville-LeVally Wear and Friction Test Machine, filling the lubricant reservoir with gear oil 150, selecting a normal load, and turning the wear test machine on to rotate the ring at 190 rpm (a sliding velocity of 35 cm/s). An initial load of 44 N was applied slowly (~5 seconds) between

the ring and block surfaces and then after the full load had been applied the ring continued to rotate against the block for 30 seconds. The load was then removed and if no galling or severe, adhesive wear had occurred, the load was increased by 44 N and reapplied for another 30 second interval. In this way the galling load test continued until a load was reached where galling between the ring and block surfaces either occurred or the applied normal load reached the load limit (3560 N) of the wear test machine. The galling load, which was characterized by a very noticeable scraping sound and a dramatic increase in the friction force, was recorded for each test.

Scanning Electron Microscopy

It was considered important to observe the wear on both the ring and the block. This was accomplished readily on the block using the Finescale comparator. On the ring, where the effect of the wear test was small, it was done by observing adjacent worn and unworn regions of selected unimplanted and implanted AISI M2 and SAE O1 tool steel rings with a Hitachi HHS-2R scanning electron microscope (SEM). The micrographs from the SEM were taken by installing a ring in the SEM's vacuum chamber so a 30 keV electron beam could be directed at the ring. Although the magnification was varied from 200x to 2000x, only micrographs taken at 200x appear in this thesis. The micrographs were then observed to identify qualitative differences between implanted and unimplanted ring surfaces that had been wear tested.

III. EXPERIMENTAL RESULTS AND DISCUSSION

AISI M2 Tool Steel

Auger Electron Spectroscopic Analysis

The nitrogen concentration vs. depth profile shown in Fig. 6 was acquired using Auger electron spectroscopy (AES) on an AISI M2 tool steel block that had been implanted with 60 keV nitrogen ions at an ion beam current density of 100 $\mu A/cm^2$ to a dose of $2x10^{17}$ N_2^+/cm^2. These are the same implantation conditions as those used on the AISI M2 tool steel rings and blocks that were wear tested. From Fig. 6, the projected range (the average depth to which ions penetrate a surface) was about 70 nm and the portion of the steel that had a relatively constant amount of nitrogen (~31 atom%) ranged from 30 nm to 110 nm below the surface. For comparison, the theoretical projected range for the same experimental implantation parameters used in this study is calculated in Appendix E from the Lindhard, Scharff and Schiott Theory.[32] The theoretical range was found to be about 55 nm for nitrogen molecules implanted into pure iron. While the theoretical projected range agrees with the experimental one to within the accuracy of the experiment and the model, it is noteworthy that an increase in the block surface temperature which may have occurred during implantation may have induced diffusion that probably caused the experimentally determined range to increase.

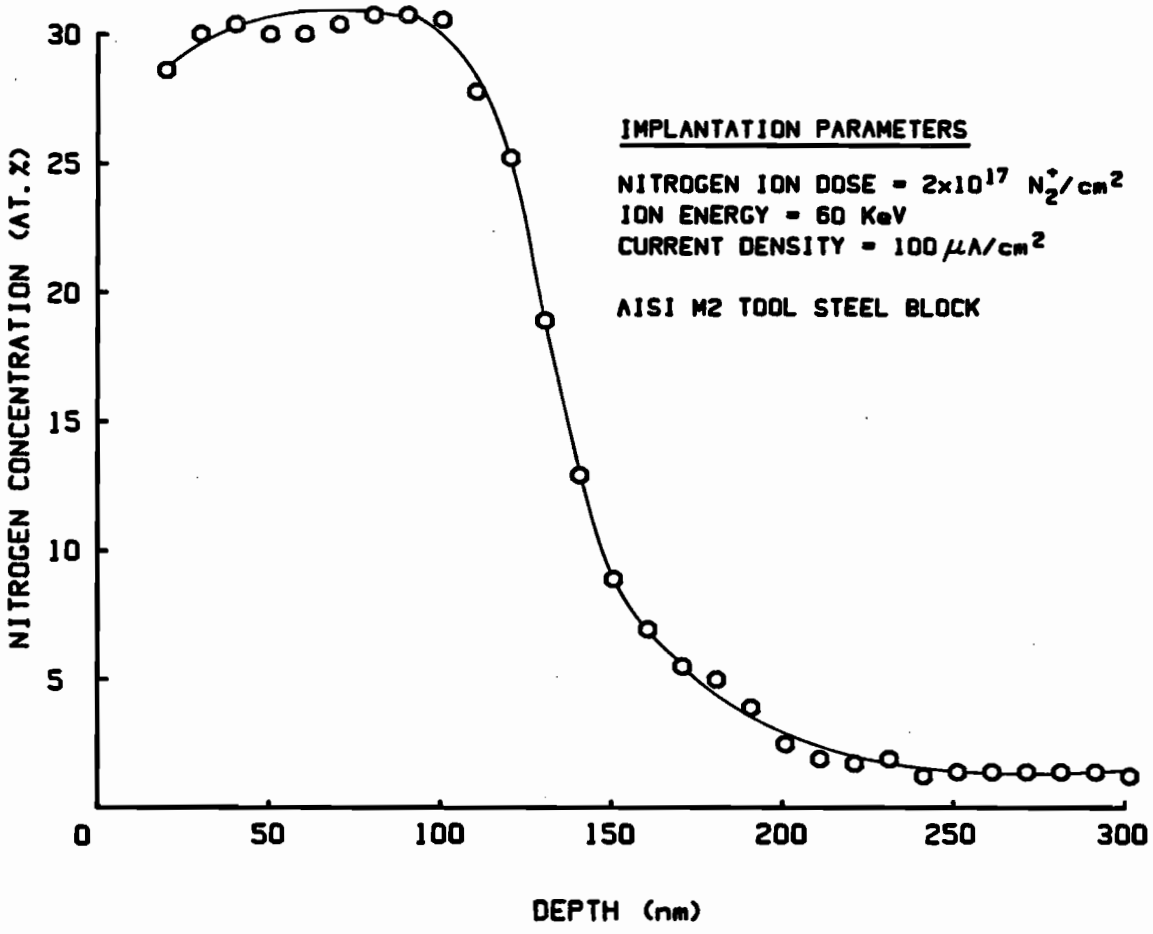

Figure 6. Nitrogen Concentration Profile in Implanted AISI M2 Tool Steel

In addition to AES analysis, x-ray photoelectron spectroscopic analysis (XPS) was performed on a nitrogen-implanted AISI M2 tool steel ring to help substantiate the accuracy of the nitrogen concentration profiles from AES analysis. Two sections of a AISI M2 tool steel ring were used, where one ring section was analyzed with AES while the other section was analyzed with XPS. The two resulting nitrogen concentration profiles were coincident within 1 atom% over the depth range where nitrogen was found. Because the independent surface analysis techniques produced similar results, the concentration profiles from AES were presumed to be accurate.

Block Wear

The effect of ion implantation on the wear behavior AISI M2 tool steel surfaces is shown in Fig. 7. The figure shows the volume of material removed from the blocks plotted against the distance that the blocks slid against the rings. The rings and blocks were implanted and wear tested at the conditions cited in Fig. 7. To obtain each data point, three wear tests were conducted and the average block wear volume was computed as the mean of these data. Scatter in the data is indicated by the error bars which represent one standard deviation from the average block wear volumes. The points representing block wear volumes from tests on unimplanted rings and blocks (⊞), show that the block wear volume increased almost linearly with sliding distance until ~4 km. At 4 km the slope of the line (equal to the wear rate) connecting the unimplanted data points (⊞), appears to decrease. The

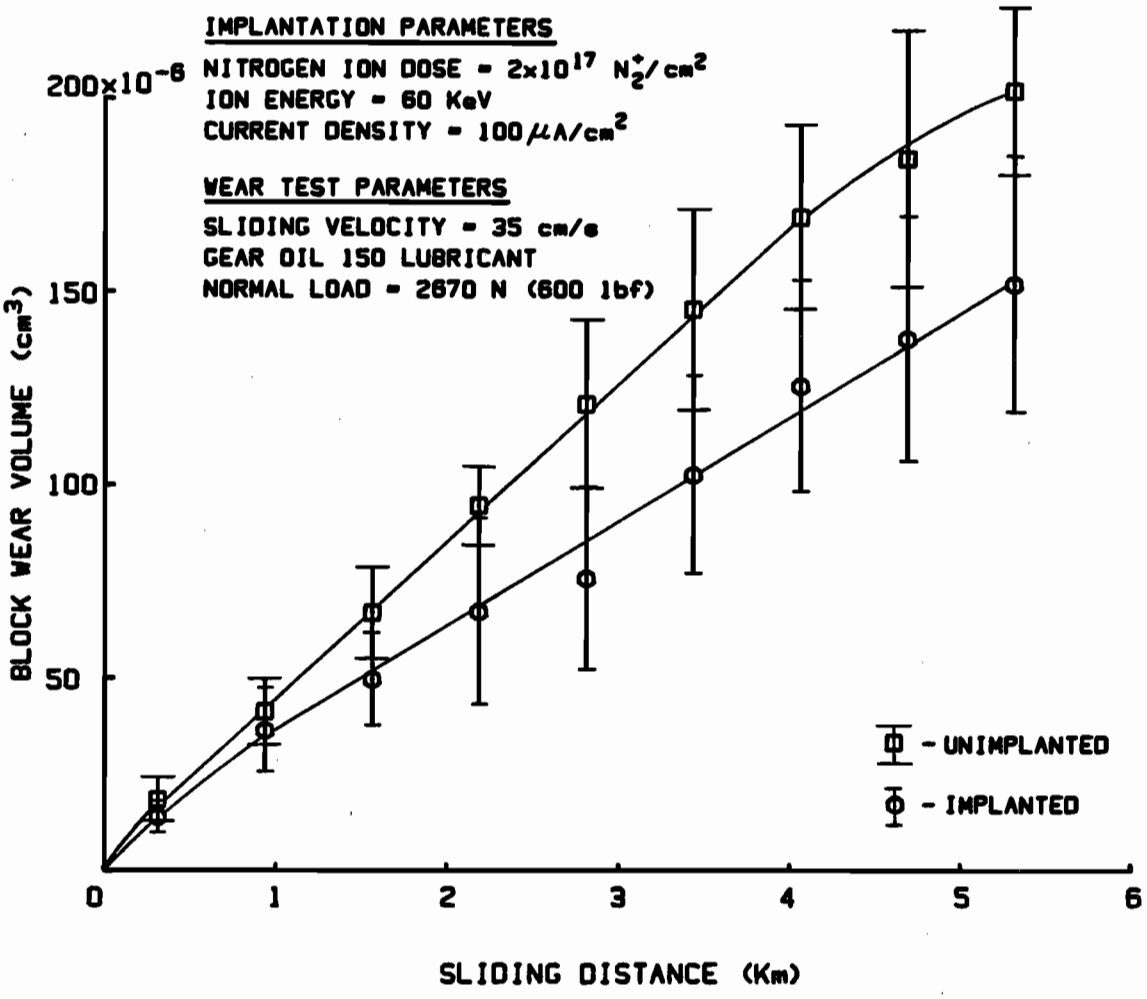

Figure 7. Effect of Nitrogen Implantation on the Sliding Wear of AISI M2 Tool Steel

data points from wear tests conducted on nitrogen-implanted rings and blocks (Φ) show that the block wear volumes at corresponding sliding distances are all less than the wear volumes determined from unimplanted sample wear tests. At the largest sliding distance of over 5 km, the implanted block wear volume was 25% less than the unimplanted wear volume. In addition, it is observed that the average slope of the line (equal to the average wear rate) connecting the implanted data points (Φ) is 2.86×10^{-10} cm^3/cm while the average slope of the line connecting the unimplanted data points (Φ) is 3.80×10^{-10} cm^3/cm.

The AISI M2 tool steel samples that were used in this study had been alloyed heavily to make them hard and wear resistant before they were implanted and the data of Fig. 7 suggest ion implantation did not improve the wear resistance as much as other researchers have observed in softer steels.[10] This result suggests that a steel that is not alloyed heavily to reduce wear is benefitted more by nitrogen ion implantation.

Friction data were recorded throughout each test. For all of the tests conducted on AISI M2 tool steel rings and blocks under lubricated conditions, the friction forces were generally less than 10% of the normal loads. There were no significant differences in friction forces seen between unimplanted and implanted samples.

Ring Wear

After wear testing AISI M2 tool steel, typical regions on the worn and unworn surfaces of one implanted and one unimplanted ring were

observed under a scanning electron microscope (SEM). The micrograph in Fig. 8a shows the surface topography of the unworn region of an unimplanted ring surface at a magnification of approximately 200x. The parallel grooves were caused by the surface finishing process used on the rings. The small white particles, running in a pattern perpendicular to the grooves, were seen on all the AISI M2 tool steel rings and probably were caused by the final grinding process. Because the width of the contact area between a ring and block during wear testing was less than the width of the ring surface, both worn and unworn adjacent regions could be observed on the same ring surface. A micrograph of the wear area of the same ring shown in Fig. 8a appears in Fig. 8b. One observes that changes occurred in the unimplanted ring surface as a result of its being worn for over 5 km of sliding distance. This observation is reached because the grooves are fewer in number in the worn region than they are in the unworn region. Similar micrographs of implanted ring unworn and worn regions appear in Figures 9a and 9b, respectively. Compared with the unimplanted ring surfaces of Figures 8a and 8b, very little difference between the worn and unworn areas of an implanted ring surface is seen in Figures 9a and 9b. Because the unimplanted ring surface was changed by the wear test and the implanted surface did not appear to be changed, more wear probably occurred on the unimplanted ring surface than on the implanted ring surface.

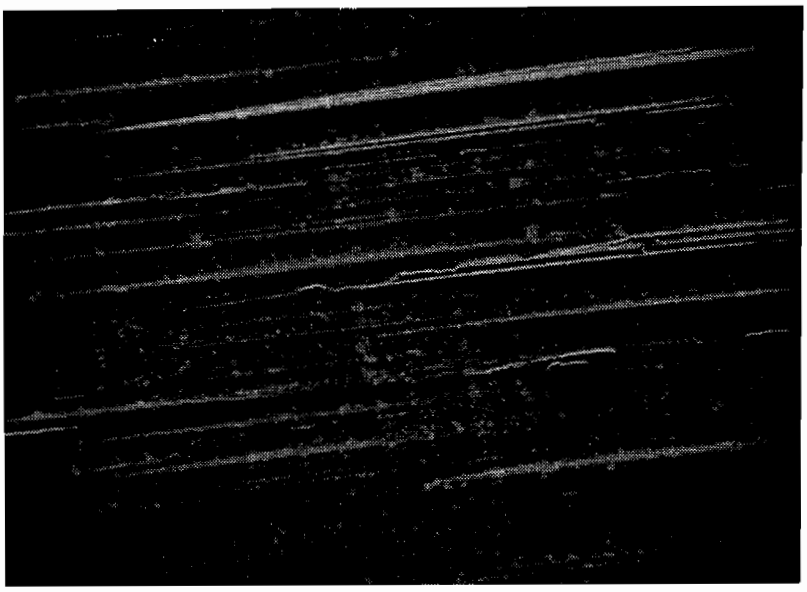

Figure 8a. SEM Micrograph of Unworn Region of Unimplanted AISI M2 Tool Steel Ring at an Approximate Magnification of 200x

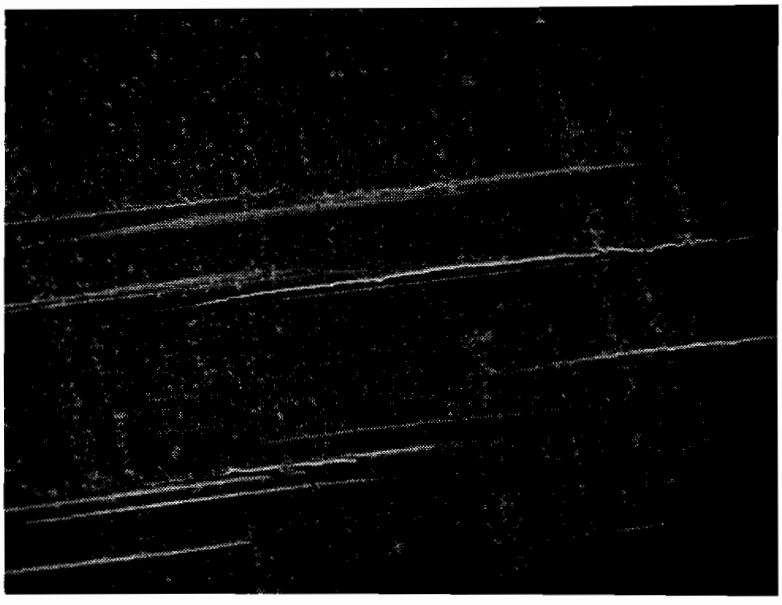

Figure 8b. SEM Micrograph of Worn Region of Unimplanted AISI M2 Tool Steel Ring at an Approximate Magnification of 200x. Wear tested under a normal load of 2670 N at a sliding velocity of 35 cm/sec in gear oil 150 lubricant for over 5 km of sliding distance.

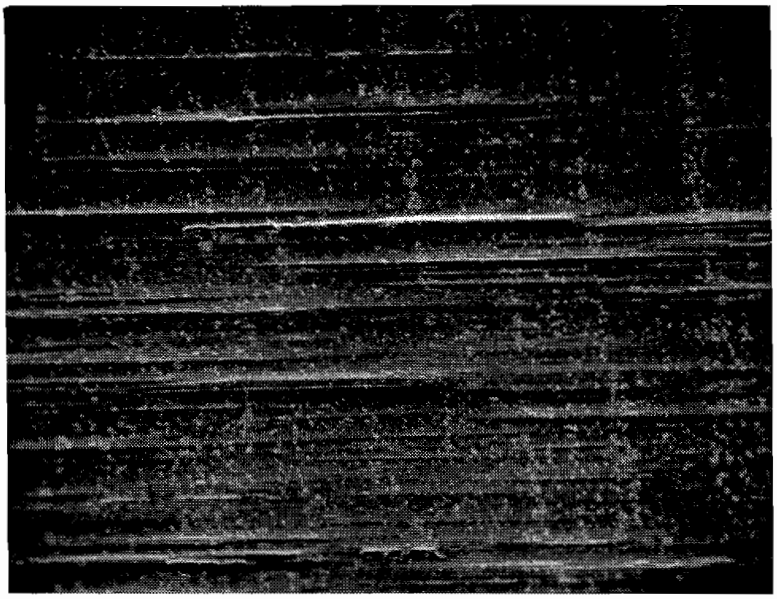

Figure 9a. SEM Micrograph of Unworn Region of Nitrogen-Implanted AISI M2 Tool Steel Ring at an Approximate Magnification of 200x. Implanted with 60 keV nitrogen ions at a current density of 100 $\mu A/cm^2$ to a dose of $2x10^{17}$ N_2^+/cm^2.

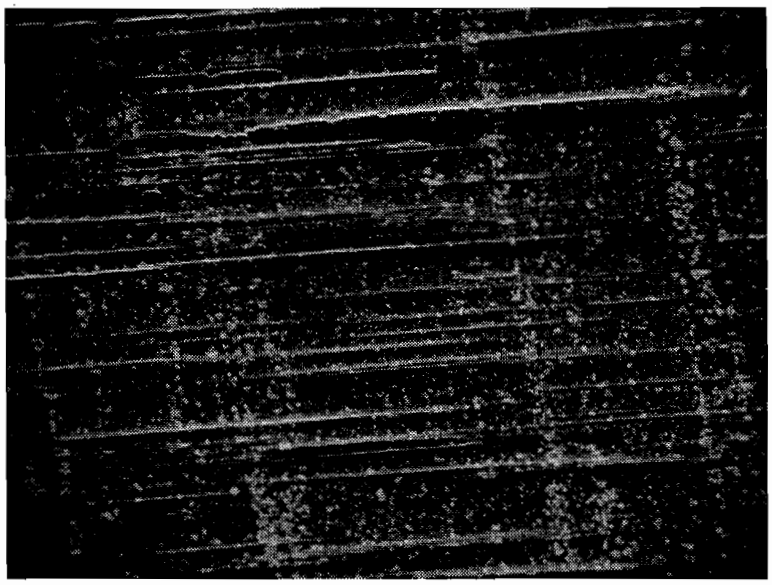

Figure 9b. SEM Micrograph of Worn Region of Nitrogen-Implanted AISI M2 Tool Steel Ring at an Approximate Magnification of 200x. Implanted with 60 keV nitrogen ions at an ion beam current density of 100 $\mu A/cm^2$ to a dose of $2x10^{17}$ N_2^+/cm^2. Wear tested under a normal load of 2670 N at a sliding velocity of 35 cm/sec in gear oil 150 lubricant for over 5 km of sliding distance.

SAE O1 Tool Steel

Auger Electron Spectroscopic Analysis

An SAE O1 tool steel block was implanted with the parameters given in Fig. 10 and analyzed with AES to obtain the nitrogen concentration vs. depth profile shown in the figure. From Fig. 10, the projected range of nitrogen in this steel was about 70 nm below the surface and the nitrogen concentration at this depth was about 29 atom%. Compared to implanted AISI M2 tool steel, SAE O1 tool steel exhibited a slightly lower peak nitrogen concentration (2 atom% less) at about the same range. It is believed that the nitrogen concentration in the SAE O1 tool steel is lower than that in the M2 tool steel because the M2 steel contained larger amounts of the nitriding materials (chromium, molybdenum, manganese, and vanadium).[33] The M2 steel therefore was better able to form such nitrogen compounds as chromium nitrides (CrN or Cr_2N). Stronger chemical binding of the nitrogen would be expected to inhibit the diffusion of nitrogen during the implantation of the AISI M2 tool steel samples, thereby causing the observed higher nitrogen concentration to occur at the shallower depths.

Block Wear

The results of wear testing unimplanted and implanted SAE O1 tool steel rings and blocks against one another appear in Fig. 11. The implantation and wear test parameters that were used for the rings and blocks also appear in this figure. Note that all of the parameters

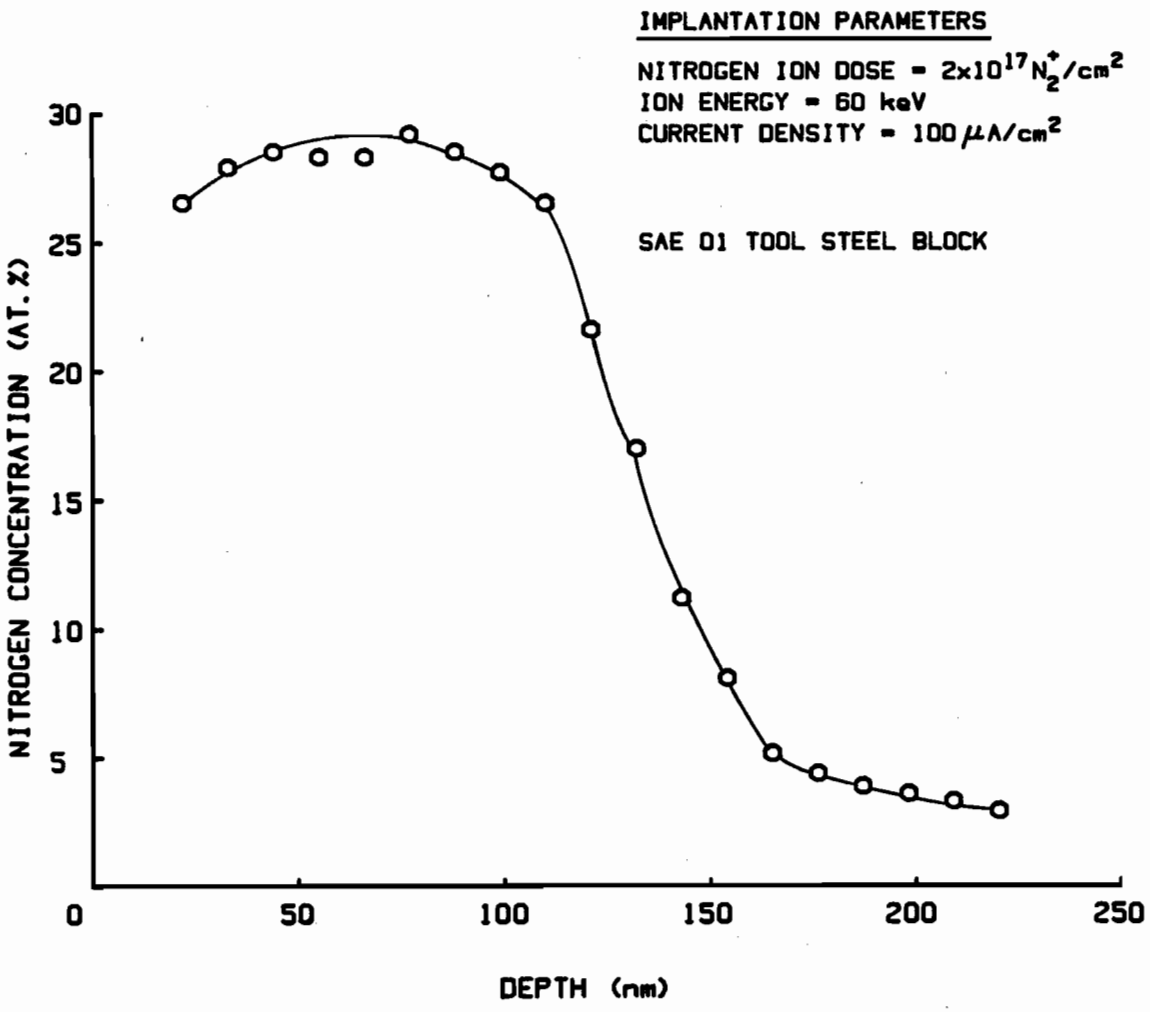

Figure 10. Nitrogen Concentration Profile in Implanted SAE 01 Tool Steel

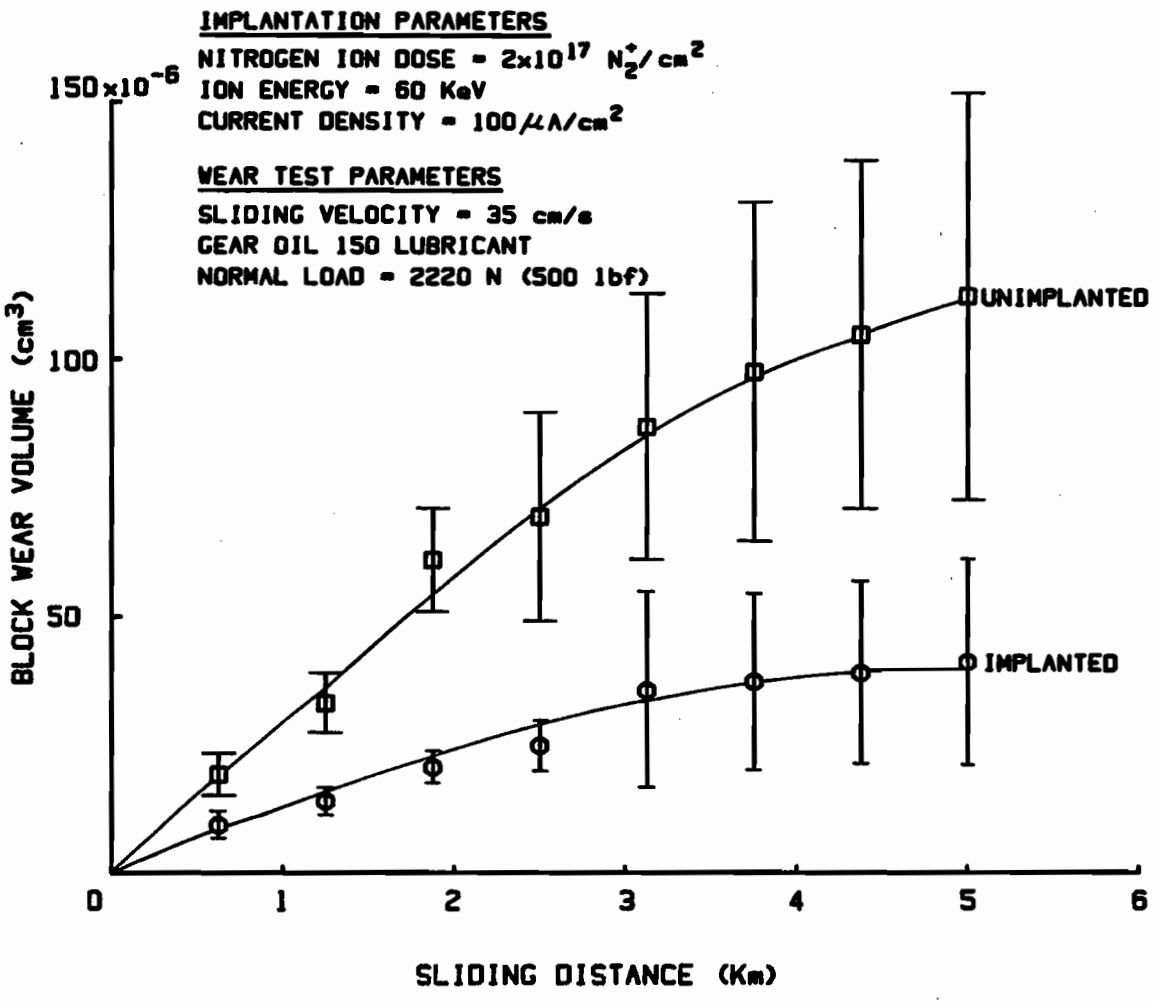

Figure 11. Effect of Nitrogen Implantation on the Sliding Wear of SAE O1 Tool Steel

except the normal load were equal to those used for the AISI M2 tool steels samples. Figure 11 shows a clear difference in block wear volumes of the implanted and unimplanted samples. After over 5 km of sliding distance, the average block wear volumes were 41×10^{-6} cm^3 for the implanted ring and block combinations and 112×10^{-6} cm^3 for the unimplanted ring and block combinations. Finally, the average wear rate of the nitrogen-implanted blocks (seen from the average slope of the curve in the figure) was 63% less than the average wear rate of the unimplanted blocks.

As with the AISI M2 tool steel samples, friction data were recorded during the wear tests conducted on the SAE O1 tool steel samples. Again no clear difference in the friction forces between implanted and unimplanted samples was observed.

Ring Wear

Figures 12 and 13 are scanning electron micrographs of a typical worn/unworn interface on the surface of unimplanted and implanted SAE O1 tool steel rings, respectively. Note the small white dots that appeared in the AISI M2 tool steel ring surfaces are not seen on the SAE O1 tool steel ring surfaces. The unworn regions appear in the upper portion of each micrograph and are differentiated from the worn regions by the presence of parallel grooves in the unworn regions caused by the machining process used to finish the rings. The worn regions (shown in the lower portion of both micrographs) of both ring surfaces contain no grooves and seem to be pitted in appearance. Because the differences

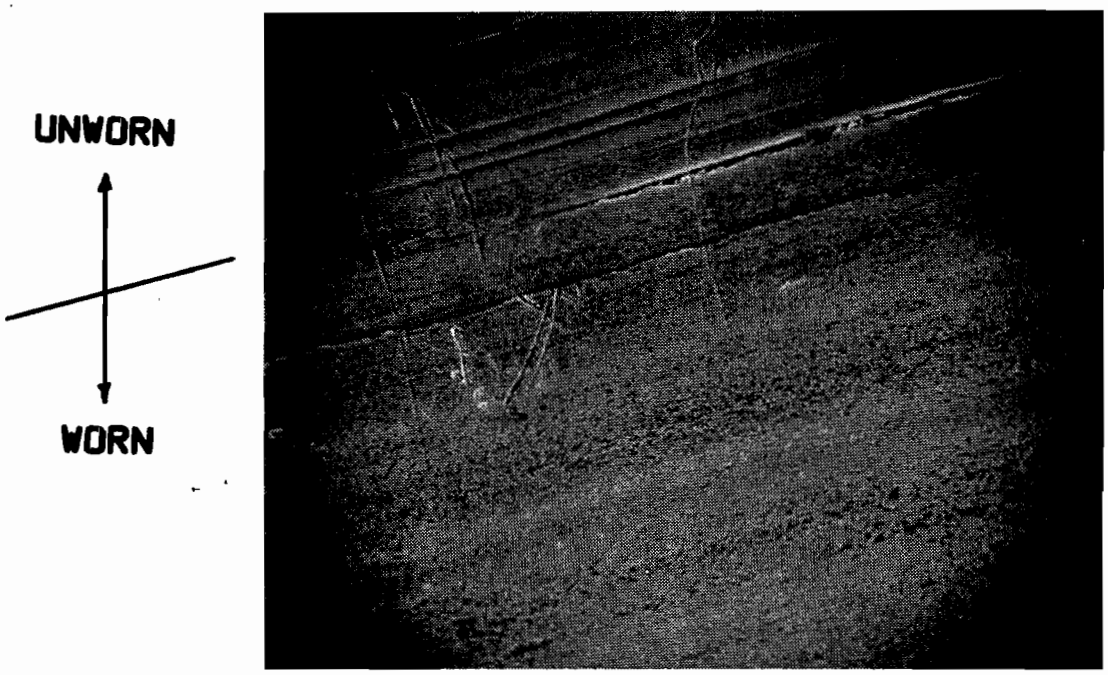

Figure 12. SEM Micrograph of Unworn/Worn Regions of an Unimplanted SAE O1 Tool Steel Ring at an Approximate Magnification of 200x. Wear tested with a normal load of 2220 N at a sliding velocity of 35 cm/sec in gear oil 150 lubricant for over 5 km of sliding distance.

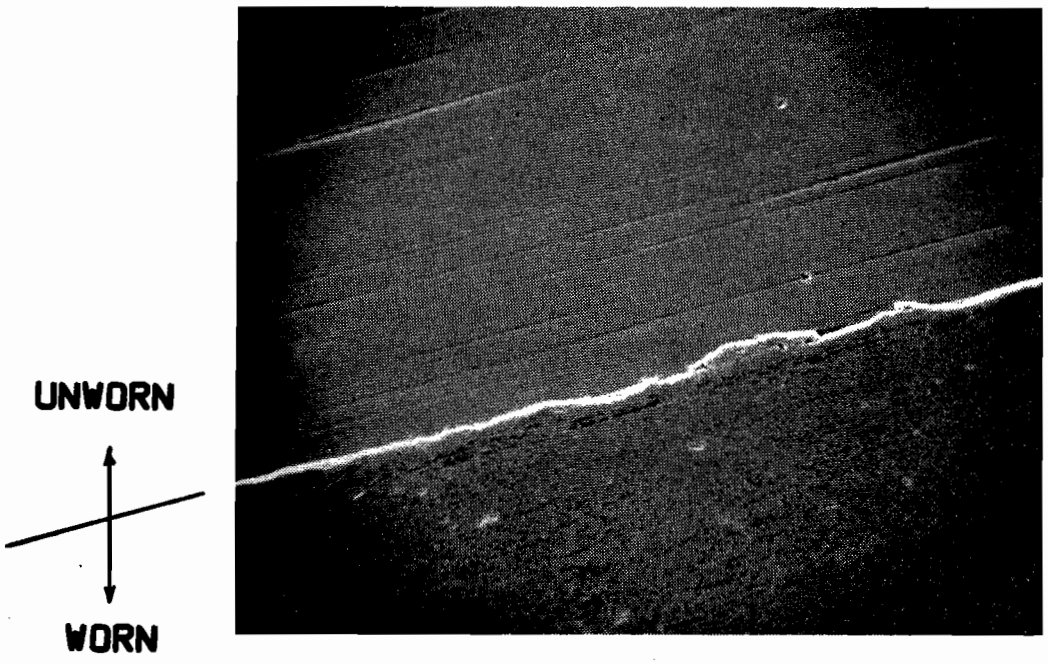

Figure 13. SEM Micrograph of Unworn/Worn Regions of a Nitrogen-Implanted SAE O1 Tool Steel Ring at an Approximate Magnification of 200x. Implanted with 60 keV nitrogen ions at a current density of 100 $\mu A/cm^2$ to a dose of 2×10^{17} N_2^+/cm^2. Wear tested under a normal load of 2220 N at a sliding velocity of 35 cm/sec in gear oil 150 lubricant for over 5 km of sliding distance.

between the unimplanted and implanted wear surfaces are not visible in the micrographs of Figures 12 and 13, no conclusions can be made concerning the possible improvement in the wear resistance of SAE O1 ring surfaces induced by nitrogen implantation.

In addition to observation of the ring surfaces with a scanning electron microscope, several ring surfaces were analyzed with a profilometer before and after wear testing to determine changes that had occurred in the surface finishes. No significant differences in the surface finishes of unimplanted and implanted rings, either before or after wear testing, were found.

AISI Type-304 Stainless Steel

Auger Electron Spectroscopic Analysis

Figure 14 shows the nitrogen concentration vs. depth profile of an AISI type-304 stainless steel block. The block was implanted with nitrogen at the conditions shown. The peak nitrogen concentration of 34 atom% occurred at a depth of 25 nm below the surface. This is a greater nitrogen concentration and it occurs at depths that are less than those found in the tool steels. This follows the theory proposed in earlier sections of this thesis (i.e., that nitrogen attaches to chromium to form chromium nitrides (CrN or Cr_2N) and this limits the diffusion of nitrogen during implantation). Because 304 stainless steel contains higher concentrations of chromium than the tool steels of this study do, one would expect thinner implanted layers and higher peak nitrogen concentrations than those found in the tool steels. For comparison, the

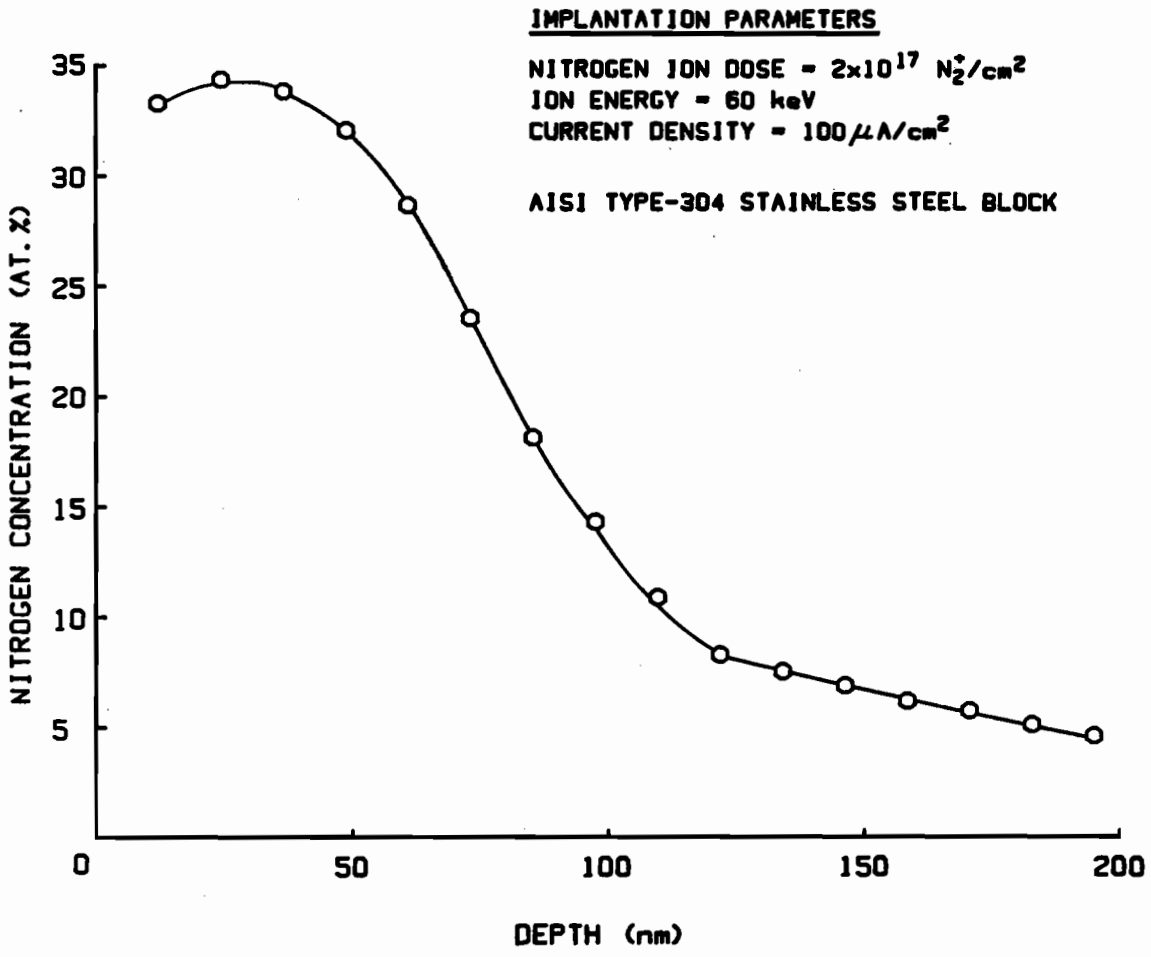

Figure 14. Nitrogen Concentration Profile in Implanted AISI Type-304 Stainless Steel

peak nitrogen concentrations and the corresponding depths at which they occurred in the implanted steels in this study are given in Table 2.

Table 2

Comparison of Nitrogen-Implanted Steels

Material	Composition (weight%)	Concentration (atom%)	Depth (nm)
SAE 01 Tool Steel	0.9%C, 1.2%Mn, 0.5%W, 0.2%V	29	70
AISI M2 Tool Steel	0.85%C, 4%Cr, 5%Mo, 6%W, 2%V	31	70
AISI Type-304 Stainless Steel	0.08%C, 19%Cr, 9%Ni	34	25

Figure 15 shows nitrogen concentration vs. depth profiles from AISI type-304 stainless steel rings that were implanted with various nitrogen ion doses and tested to determine galling loads. The rings were implanted with 60 keV nitrogen ions at a rate of 100 $\mu A/cm^2$. Note the nitrogen concentration profiles in Fig. 15 are from rings that had been tested while all previously shown profiles had been obtained before testing of the implanted rings. The figure shows that as the nitrogen dose is increased, both the concentration and the penetration depth of the nitrogen increase. For example, at a dose level of $5x10^{15}$ N_2^+/cm^2 the peak nitrogen concentration of 4 atom% occurs 30 nm below the surface while a dose level of $75x10^{15}$ N_2^+/cm^2 produces a peak nitrogen concentration of 18 atom% at an average depth of 50 nm. It is observed at the highest dose level of $75x10^{15}$ N_2^+/cm^2 that the nitrogen

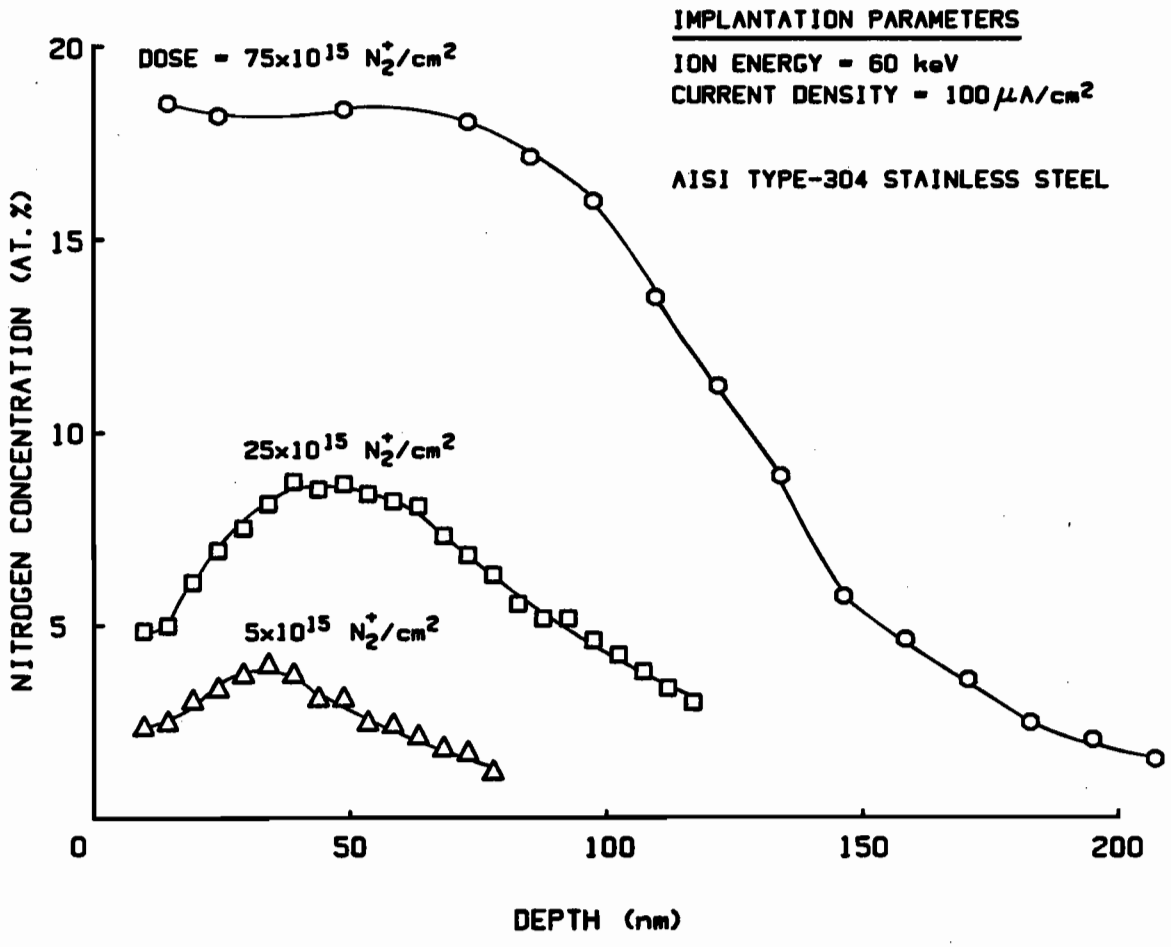

Figure 15. Nitrogen Concentration Profiles in Implanted and Worn AISI Type-304 Stainless Steel Rings

concentration is relatively constant from near the surface to about 75 nm below the surface.

Effect of Nitrogen Ion Dose Variation on Galling Load

The galling loads measured on several rings and block pairs implanted with 60 keV nitrogen ions at a current density of 100 $\mu A/cm^2$ and various dose levels are shown in Fig. 16. All the galling load tests were performed in gear oil 150 lubricant at a sliding velocity of 35 cm/sec. The galling loads from the implanted samples were normalized with respect to the galling load for unimplanted samples. To find the unimplanted galling load, four tests were performed on unimplanted AISI type-304 stainless steel rings and blocks. All four tests yielded a galling load of 90 N(20lb_f). As shown in Fig. 16, the galling load (load-bearing capacity) of nitrogen implanted ring and block surfaces was increased to a value over 40 times the capacity of unimplanted ring and block surfaces. The nitrogen ion dose which caused the largest increase in the galling load was 2.5×10^{16} N_2^+/cm^2. Unfortunately, with the wear and friction test machine that was used, some implanted test samples could not be tested at high enough loads to cause the occurrance of galling. The data point at the dose level of 2.5×10^{16} N_2^+/cm^2 (δ) represents a test in which the load limit of the test machine was not high enough and the ring and block surfaces did not gall at any applied load. Figure 16 shows that peak galling loads are reached at implanted-nitrogen doses ranging from about 2×10^{16} N_2^+/cm^2 to 7×10^{16} N_2^+/cm^2. As the nitrogen dose is increased to values above 7×10^{16}

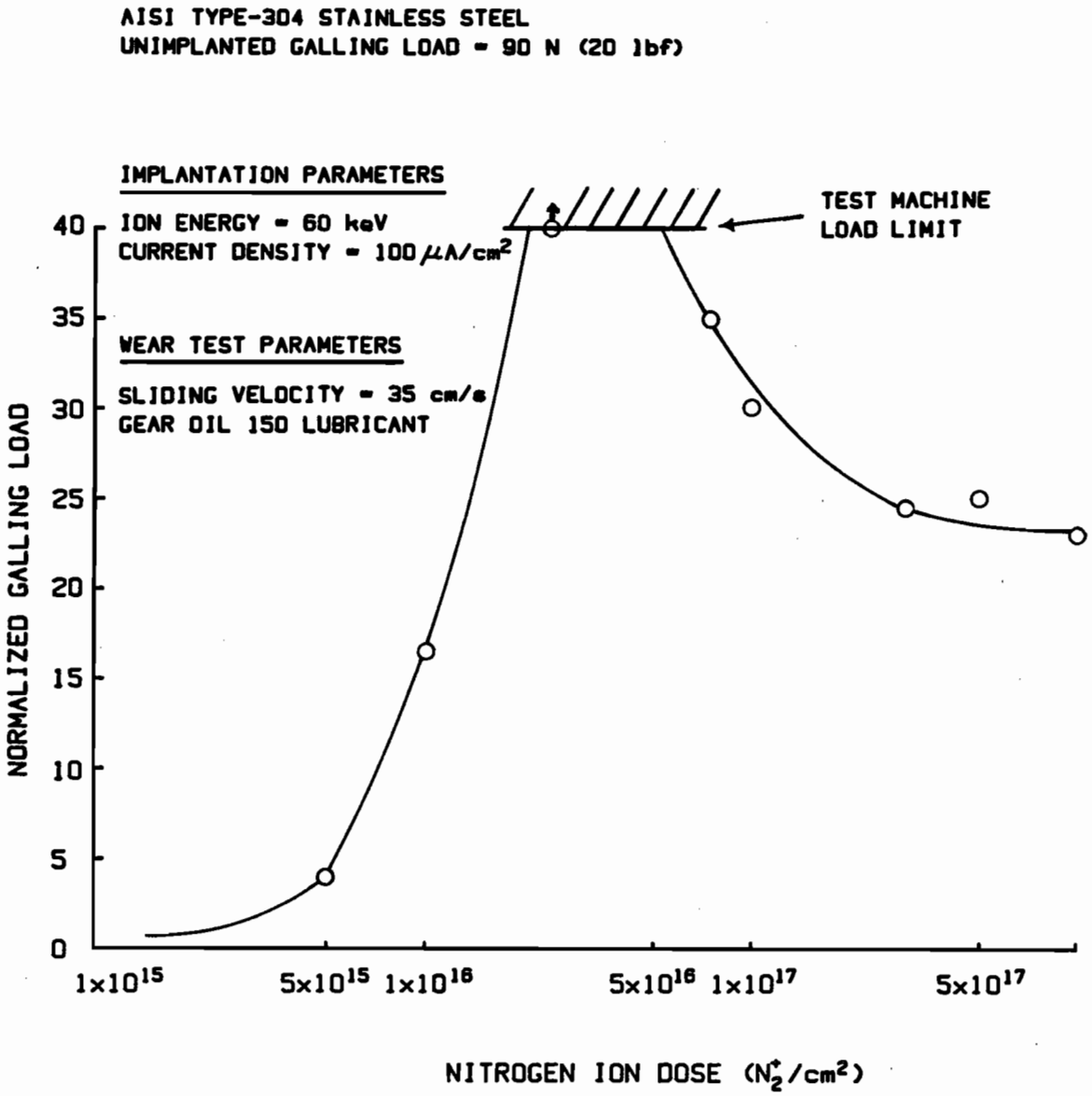

Figure 16. Galling Loads of Nitrogen-Implanted Samples Normalized to the Unimplanted Galling Load for Various Ion Doses

N_2^+/cm^2, the measured galling load at a dose of $1x10^{18}$ N_2^+/cm^2 decreased to a value 23 times the galling load of unimplanted samples. It is not known why this occurred.

Several rings and blocks were implanted with 60 keV nitrogen ions at current densities (implantation rates) greater than 100 $\mu A/cm^2$ to learn if samples implanted at such dose levels would still exhibit higher galling loads than unimplanted samples. The curve that represents the galling load data from AISI type-304 stainless steel samples implanted at 100 $\mu A/cm^2$ is repeated in Fig. 17 along with galling load curves from samples implanted at 300 $\mu A/cm^2$ and 1500 $\mu A/cm^2$. Because nitrogen implantation had the greatest effect on the galling load at nitrogen doses below $1x10^{17}$ N_2^+/cm^2, only dose values below this level were used in the tests at the higher current densities. It appears from Fig. 17 that to obtain over a forty-fold increase in the galling load at current densities of 300 $\mu A/cm^2$ and 1500 $\mu A/cm^2$, AISI type-304 stainless steel samples must be implanted at nitrogen dose levels near $7.5x10^{16}$ N_2^+/cm^2. Because sample temperature was not rigidly controlled during implantation, retained doses may not have been exactly equal to implanted nitrogen doses (especially for samples implanted at the higher current densities) due to the possibility of nitrogen diffusion occurring at elevated sample temperatures. Therefore, it cannot be stated conclusively that the nitrogen dose needed to obtain a maximum galling load is $7.5x10^{16}$ N_2^+/cm^2 at current densities of 300 $\mu A/cm^2$ and 1500 $\mu A/cm^2$. As long as the sample temperature is rigidly controlled at low temperatures ($<100\ ^{o}C$) during nitrogen ion implantation, the galling load of AISI type-304 stainless steel samples is probably independent of ion beam current density.

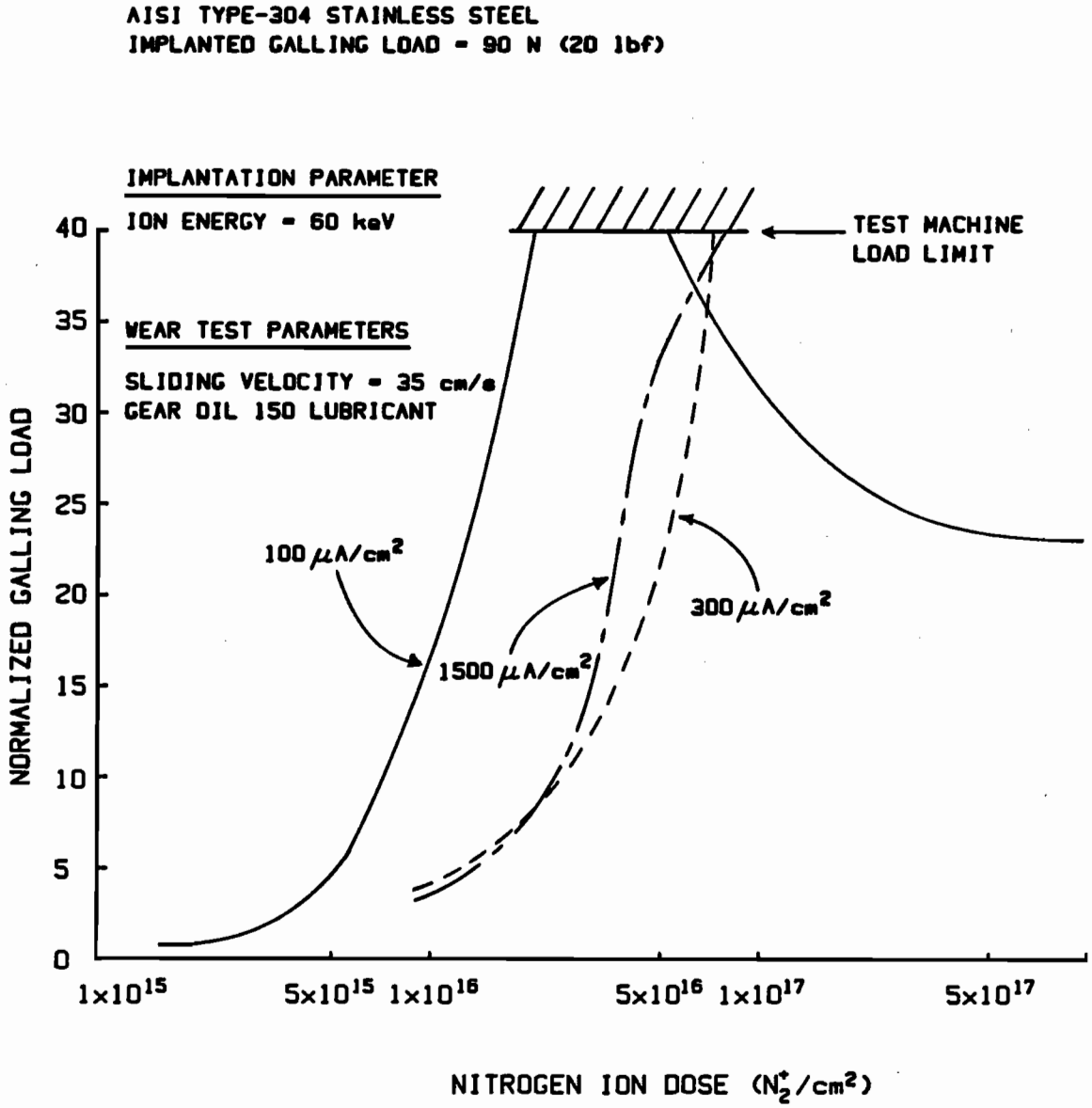

Figure 17. Galling Load Curves of Nitrogen-Implanted Samples Normalized to the Unimplanted Galling Load for Various Ion Doses and Current Densities

Because dark streaks were observed on a few nitrogen-implanted AISI type-304 stainless steel ring surfaces that had been tested with significant loads (3560 N), both nitrogen and carbon concentration profiles were studied from a tested ring and block pair in which the ring demonstrated this phenomenon. Figure 18 shows these concentration profiles in the analyzed AISI type-304 stainless steel block implanted with 60 keV nitrogen ions at a current density of 300 $\mu A/cm^2$ to a dose of $1x10^{17}$ N_2^+/cm^2 and tested in gear oil 150 lubricant against the ring implanted at equal conditions. The profiles were obtained from an implanted region on the block that had not been loaded. The nitrogen concentration profile peaks at 27 atom% 50 nm below the block surface and appears to be rather typical when compared with a previous profile (Fig. 14). The carbon concentration in the figure shows high carbon content (7 atom%) near the block surface which may be due to gear oil 150 residue that formed on the surface during the galling load test. At depths greater than 25 nm, the carbon concentration decreases to a value close to or below the bulk carbon concentration of AISI type-304 stainless steel (0.08 atom%). In contrast to the profiles in Fig. 18, Fig. 19 shows the nitrogen and carbon concentration profiles of the ring from a region that had been significantly loaded. The very different nitrogen profile in the ring (compared to the one from the block) never reaches nitrogen concentrations above 10 atom% and is relatively constant up to a depth of 250 nm. The carbon concentration profile in the ring is also very different from the one in the block and is shown to be very high (20 atom%) near the ring surface and reach about the same nitrogen concentration level (7.5 atom%) at depths greater than 75 nm. The differences in the carbon and nitrogen concentration observed

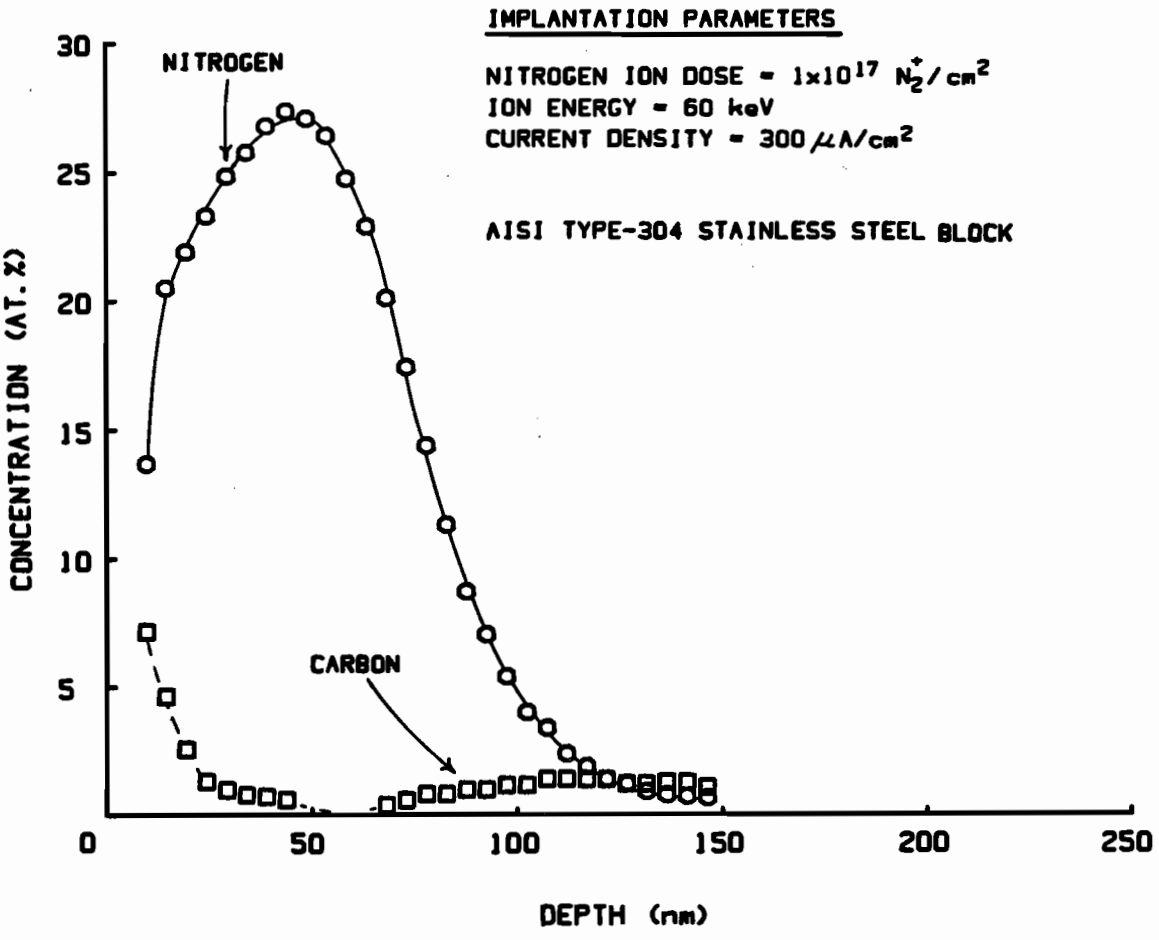

Figure 18. Nitrogen and Carbon Concentration Profiles in Unworn Region of Tested AISI Type-304 Stainless Steel Block

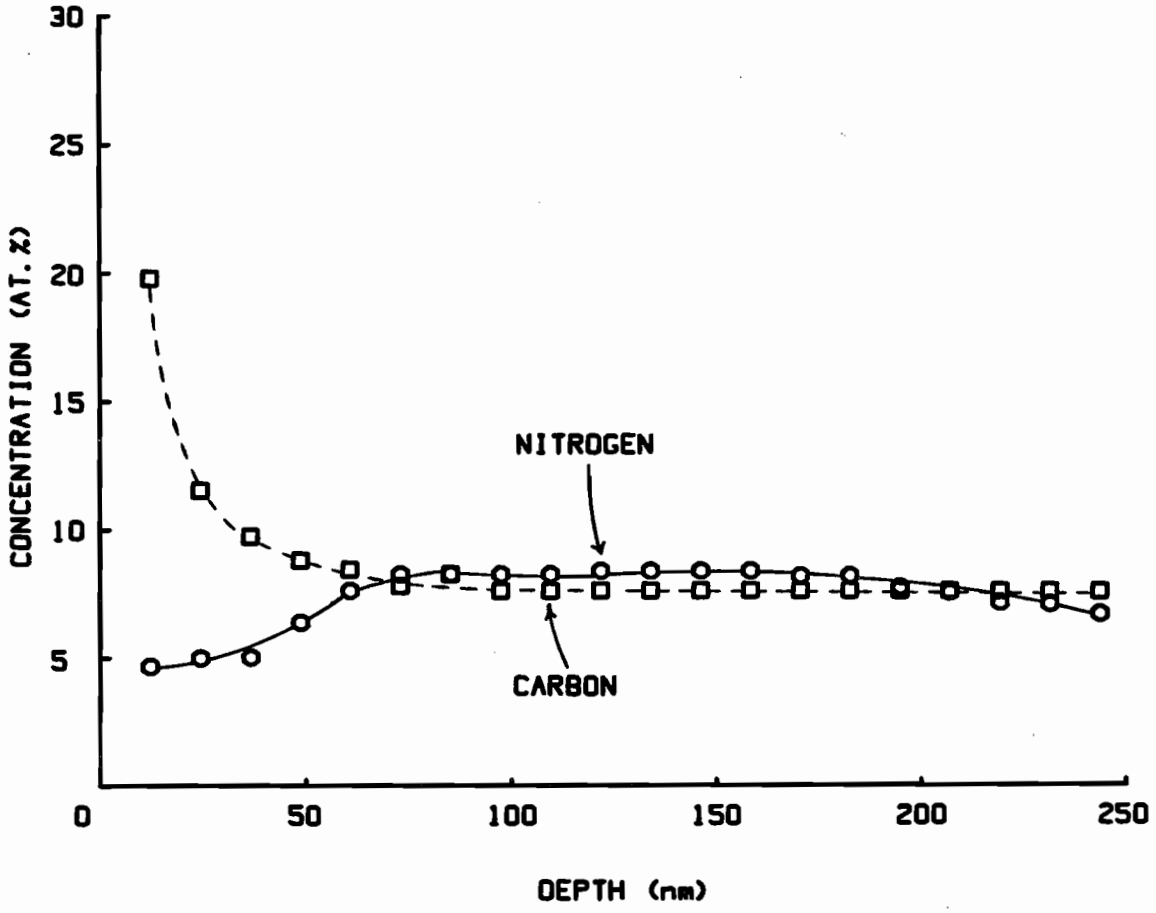

Figure 19. Nitrogen and Carbon Concentration Profiles in Worn Region of Tested AISI Type-304 Stainless Steel Ring

between the ring and the block may be due to what has been called tribo-enhanced diffusion.[34] It is postulated that the elevated surface temperature and the surface deformation that occurred during the galling load test, caused nitrogen to migrate inward from the ring surface so that a relatively "flat" profile and low nitrogen concentrations (7.5 atom%) occurred. The same mechanisms probably caused carbon (derived from the lubricant) to diffuse to more than 250 nm into the ring surface. This high carbon content (>7.5 atom%) in the near-surface layers of the ring may have aided in lubricating the ring and block interface during the galling load test.

Effect of Nitrogen Ion Energy Variation on Galling Load

Figure 20 shows how the galling load of implanted AISI type-304 stainless steel rings and blocks changed with implanted ion energy. The samples were implanted at a current density of 300 $\mu A/cm^2$ to a dose of $5x10^{16}$ N_2^+/cm^2. The dose was chosen below what appeared from previous results to be the optimum dose at the selected current density in order to remain within the load range of the wear and friction test machine. The tests were conducted with the wear test parameters given in Fig. 20 and the galling loads were normalized with the unimplanted galling load of 90 N ($20lb_f$). As shown, the ion energy resulting in the largest normalized galling load of about 21 at the given implantation parameters, was 70 keV. The normalized galling load is found to decrease at higher energies.

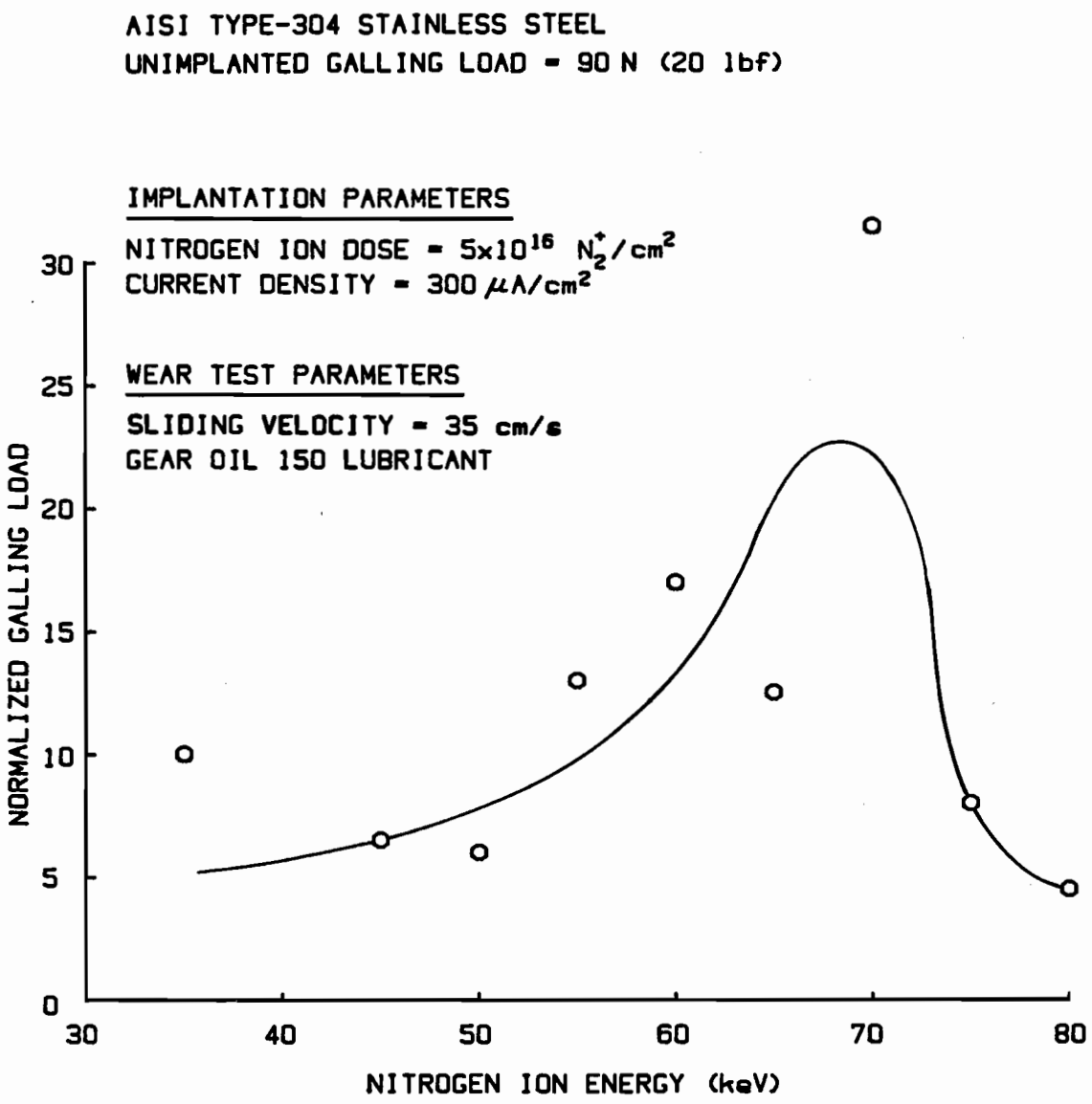

Figure 20. Galling Loads of Nitrogen-Implanted Samples Normalized to the Unimplanted Galling Load for Various Ion Energies

The large increases in the load-bearing capacity of nitrogen implanted AISI type-304 stainless steel that were seen is most likely due to the formation of hard chromium nitrides (CrN or Cr_2N). Although no tests were performed in this study to confirm the formation of chromium nitride in nitrogen-implanted type-304 stainless steel, several publications support its formation.[1,5,10,35-38] Because iron nitrides are generally not formed in type-304 stainless steel implanted to nitrogen doses less than $1x10^{17}$ N_2^+/cm^2,[17,37] further support is given to the conclusion that the increase in galling loads was due only to chromium nitride formation.

Diffusion-Enhanced Implantation

Much greater depths than those normally observed with 60 keV nitrogen ions may be achieved by implanting AISI type-304 stainless steel surfaces at high dose rates that induce high surface temperatures (> 450 ^oC). An example of the change induced in nitrogen concentration vs. depth profiles by changes in incident ion current density is shown in Fig. 21. To obtain the results presented in the figure, three AISI type-304 stainless steel blocks were implanted with 60 keV nitrogen ions at ion beam current densities of 10 $\mu A/cm^2$, 100 $\mu A/cm^2$ and 1500 $\mu A/cm^2$ to a dose of $1x10^{17}$ N_2^+/cm^2. During implantation, the samples were mounted in a water-cooled fixture. Throughout each implantation event, the implanted block surface temperatures were measured and recorded. These surface temperature vs. time plots appear in Appendix A. The peak surface temperature that was reached during implantation of each sample

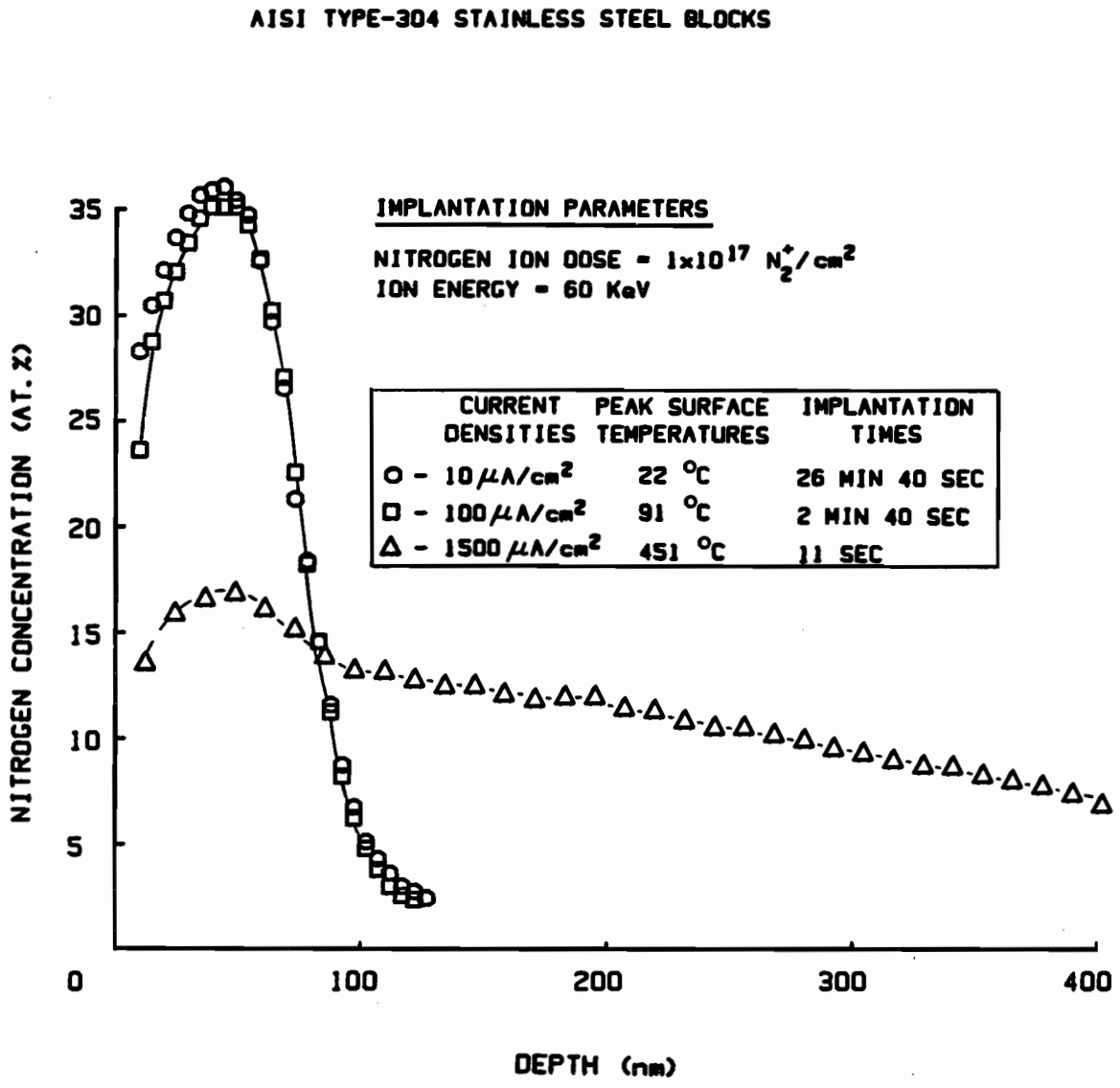

Figure 21. Diffusion-Enhanced Implantation in AISI Type-304 Stainless Steel Blocks

and the length of time that each sample was exposed to the ion beam are given in Fig. 21. Hereafter, the samples implanted with the ion beam current densities of 10 $\mu A/cm^2$, 100 $\mu A/cm^2$ and 1500 $\mu A/cm^2$ will be referred to as Sample 1, Sample 2 and Sample 3, respectively. The data representing Sample 1 (o) and Sample 2 (□) produced almost identical nitrogen concentration profiles. The peak nitrogen concentration of both samples is about 36 atom% and occurs 50 nm below the sample surfaces. The nitrogen concentrations of both sample surfaces are observed to become negligible beyond about 120 nm. Note that the surface temperature of neither of these samples rose substantially during implantation. In contrast, Sample 3 exhibits the dramatically different nitrogen concentration profile, shown in Fig. 21. In this case the peak nitrogen concentration is 17 atom% and it occurs about 50 nm below the sample surface. Not only is the peak nitrogen concentration of Sample 3 much lower than that of the other two samples, but the depth to which the nitrogen penetrates is much greater. For example at a depth of 200 nm, Sample 3 shows a nitrogen concentration of 12 atom% while Samples 1 and 2 exhibit no observable nitrogen at this depth. In this experiment, the surface of Sample 3 reached a temperature of ~450 ^{o}C during the 11 second exposure to the high current density ion beam that was required to introduce the desired dose.

In some materials that are implanted with nitrogen at high temperatures, the nitrogen is not retained. For example, it is known that pure iron implanted with nitrogen above 300 ^{o}C retains very little nitrogen.[14] It is considered likely that Sample 3 retained the nitrogen because chromium nitrides (CrN and Cr_2N) were formed. The chromium nitrides that were probably formed may also have served as a barrier to

outward diffusion of the free nitrogen (nitrogen not chemically bound) thus enhancing diffusion inward.

The nitrogen in Sample 3 migrated inward and in order to know if this was due entirely to thermal equilibrium diffusion, Fick's Law was used in the form of Eq. 2,

$$\frac{\Delta d_N}{\Delta t} = -D_N \frac{dn}{dX} \qquad (2)$$

where $\Delta d_N/\Delta t$(atoms/cm^{2}sec) is the nitrogen diffusion rate, D_N(cm^2/sec) is the thermal diffusion coefficient of nitrogen in AISI type-304 stainless steel and dn/dx(atoms/cm^4) is the gradient of nitrogen atom concentration in the x-direction measured inward from the sample surface. Because the thermal diffusion coefficient decreases exponentially as the temperature decreases, the thermal diffusion becomes relatively insignificant at temperatures below 400 ^{o}C.[4] Therefore it was logical to consider only the time at which Sample 3 was between 400 ^{o}C and 450 ^{o}C (~5 seconds). The diffusion coefficient for nitrogen in AISI type-316 stainless steel at the corresponding mean temperature (425 ^{o}C) was determined by interpolation of the data of Ref. 4. The diffusion coefficient of nitrogen in AISI type-316 stainless steel was used rather than in AISI type-304 because data for 304 stainless steel could not be found and these two steels are similar. The concentration gradient of nitrogen atoms was estimated conservatively using the nitrogen concentration profile of Sample 1 in Fig. 21 between the depths of 60 nm and 90 nm to be $-9.8\text{x}10^{27}$ atoms/cm^4. The total number of atoms that should have diffused beyond 100 nm was estimated using Eq. 2 and was found to be about three orders of magnitude less than the number determined by integrating under the

nitrogen concentration profile for Sample 3 beyond 100 nm. It is therefore argued that thermal equilibrium diffusion alone is not responsible for the migration of the nitrogen. This result is also supported by Ref. 10.

It is believed that the additional mechanisms that facilitated nitrogen migration inward involved the production and migration of two defects during implantation.[39] These defects were: i) interstitials (extra atoms forced into crystal lattice regions) and ii) vacancies (unoccupied lattice sites). Large numbers of both vacancies and interstitials are produced by ion implantation. According to Ref. 40 a sufficiently high temperature causes the defects to migrate through lattices and this in turn induces mass transport (diffusion). This effect is called radiation-enhanced diffusion. Based on evidence obtained from nickel foils,[40] radiation-enhanced diffusion effects dominate at temperatures less than ~750 ^{o}C and the effects diminish with decreasing temperature to ~200 ^{o}C. Below ~200 ^{o}C radiation-enhanced diffusion effects are relatively independent of temperature and only a function of the production rate of defects. Assuming that implanted nitrogen diffuses in AISI type-304 stainless steel in a manner similar to the way it does in nickel, the diffusion rates suggested by the data of Fig. 21 can be explained by radiation-enhanced diffusion effects. The diffusion of nitrogen was not seen in Samples 1 and 2 because the diffusion coefficients due to defect production and migration corresponding to the implantation temperatures of these samples were too small to cause significant diffusion of nitrogen. In contrast, the peak surface temperature of Sample 3 was higher (450 ^{o}C) and this enabled the

higher diffusion coefficient which facilitated more rapid nitrogen diffusion.

No literature was found on the theoretical determination of nitrogen concentration profiles in AISI type-304 stainless steel that had been implanted at high current densities (1500 $\mu A/cm^2$) and high temperatures (450 ^{o}C). The mathematical description of this would be based on effects of radiation-enhanced diffusion which is somewhat complicated. The reader is referred to References 39-41 for more mathematical detail on radiation-enhanced diffusion.

IV. CONCLUSIONS

The following conclusions are drawn from this research:

1. The broad beam, high current density implantation system that has been designed to implant non-semiconducting materials can be operated for extended periods of time at voltages up to 80 kV and current densities well over 1500 $\mu A/cm^2$. The system operates efficiently on argon, acetylene, oxygen and diborane.
2. When AISI M2 tool steel, SAE O1 tool steel or AISI type-304 stainless steel are subjected to identical implantation conditions, the AISI type-304 stainless steel exhibits the largest peak nitrogen concentration at the smallest depth (34 atom% at 25 nm). It is postulated that the high concentration (19 atom%) of chromium in AISI type-304 stainless steel facilitates the formation of chromium nitrides (CrN and Cr_2N)[1,5,7,34-36] which may inhibit radiation-enhanced diffusion of nitrogen during nitrogen implantation. Therefore, generally more nitrogen diffusion appears to occur in nitrogen-implanted steels that have less chromium available to bind with nitrogen.
3. For AISI M2 tool steel samples that have been implanted with nitrogen and slid over a 5 km distance while lubricated, a 25% decrease in wear is observed in comparison to

unimplanted samples. This occurs when the samples have been implanted with 60 keV nitrogen ions at an ion beam current density of 100 $\mu A/cm^2$ and a dose of $2x10^{17}$ N_2^+/cm^2.

4. For SAE 01 tool steel samples, nitrogen implantation induces a 63% reduction in wear for samples implanted with 60 keV nitrogen ions at a current density of 100 $\mu A/cm^2$ to a dose of $2x10^{17}$ N_2^+/cm^2. To observe the reduction in wear, similarly treated samples are forced against one another with a load of 2220 N while under lubricated conditions over a 5 km sliding distance.

5. The load-bearing capacity of an AISI type-304 stainless steel surface is improved to a level of over 40 times the capacity of unimplanted surfaces when it is implanted with 60 keV nitrogen ions at an ion beam current density of 100 $\mu A/cm^2$ and a dose near $2.5x10^{16}$ N_2^+/cm^2. When the ion beam current density is increased to 300 $\mu A/cm^2$ and 1500 $\mu A/cm^2$ at the same ion energy, the dose necessary to achieve the same increase in the load-bearing capacity is nearer $1x10^{17}$ N_2^+/cm^2. This current density-induced change in the optimum dose is probably due to some nitrogen diffusion occurring at the higher ion beam current densities. The optimum ion beam energy necessary to achieve the maximum increase in the load-bearing capacity of this same steel appears to be near 70 keV.

6. Diffusion-enhanced implantation of nitrogen in AISI type-304 stainless steel is induced when a sample (in good thermal contact with a heat sink) is implanted with 60 keV nitrogen

ions at a current density near 1500 $\mu A/cm^2$ and a dose of $1x10^{17}$ N_2^+/cm^2. At these conditions, a high nitrogen concentration (10 atom%) is forced to depths over 300 nm below the sample surface. The peak surface temperature during implantation at these conditions is near 450 ^oC and this enables the nitrogen to diffuse inward by defect production and migration mechanisms. The chromium in the AISI type-304 stainless steel probably forms chromium nitrides (CrN and Cr_2N) with the nitrogen which may create a shallow barrier (at 50 nm below the surface) that inhibits the outward diffusion of the chemically-unbound nitrogen. In contrast, when samples are implanted at lower current densities of 10 $\mu A/cm^2$ and 100 $\mu A/cm^2$ with all other parameters remaining unchanged, the surfaces reach temperatures no higher than 95 ^oC and no significant diffusion of nitrogen is observed. This is supported by observing no significant nitrogen concentrations at depths greater than 120 nm in samples implanted at the lower dose rates.

REFERENCES

1. Hirvonen, J. K., et. al., "Improvement of Metal Properties by Ion Implantation", Thin Solid Films, Vol 63, 1979, pp. 6,7.

2. Townsend, P. D., J. C. Kelly, and N. E. W. Hartley, Ion Implantation, Sputtering and their Applications, Academic Press Inc., London England, 1976, p. 8.

3. Butler, J. W., "Ion Implantation Science and Technology", Contribution to The Use of Ion Implantation for Materials Processing, NRL Memorandum Report 4341, Oct. 6, 1980, Table 1, p. 8.

4. Hirvonen, J. and A. Anttila, "Annealing Behavior of Implanted Nitrogen in AISI 316 Stainless Steel", Appl. Phys. Lett., 46(9), 1 May 1985, pp. 835-836.

5. Yost, F. G., et. al., "The Effects of N^+ Implantation on the Wear and Friction of Type 304 and 15-5 ph Stainless Steels", Thin Solid Films, 73(1980), pp. 285-288.

6. Dearnaley, G. and N. E. W. Hartley, "Ion Implantation into Metals and Carbides", Thin Solid Films, 54(1978) pp. 215-232.

7. Hirvonen, J. K., "Ion Implantation in Tribology and Corrosion Science", J. Vac. Sci. Technol., 15(5), Sept/Oct. 1978, pp. 1662-1668.

8. Koves, G., Materials for Structural and Mechanical Functions, Hayden Book Company, Inc., New York, 1970, p. 344.

9. Singer, I. L., R. N. Bolster, C. A. Carosella, "Abrasive Wear Resistance of Titanium-and Nitrogen-Implanted 52100 Steel Surfaces", Thin Solid Films, 73(1980) pp. 285-288.

10. Dimigen, H. and K. Kobs, "Wear Resistance of Nitrogen-Implanted Steels", Materials Science and Engineering, 69 (1985) pp. 181-190.

11. Carosella, C. A. and C. R. Gossett, "Function and Wear Reduction of Bearing Steel Via Ion Implantation", Contribution to The Use of Ion Implantatiion for Materials Processing, NRL Memorandum Report 4341, Oct. 6, 1980, pp. 33-47.

REFERENCES (cont'd)

12. Picraux, S. T., and L. E. Pope, "Tailored Surface Modification by Ion Implantation and Laser Treatment", Science, Vol 226, Number 4675, 9 November 1984, pp. 615-622.

13. Bolster, R. N., and I. L. Singer, "Surface Hardness and Abrasion Wear Resistance of Ion-Implanted Steels", Contribution to The Use of Ion Implantation for Materials Processing, NRL Memorandum Report 4341, Oct. 6, 1980, pp. 49-56.

14. Goode, P. D. and I. J. R. Baumvol, "The Influence of Ion Implantation Parameters on the Surface Modification of Steels", Nucl. Instrum. Method, 189(1981), pp. 161-168.

15. Lo Russo, S., et. al., "Effect of Nitrogen Ion Implantation on the Unlubricated Sliding Wear of Steels", Appl. Phys. Lett. 34(10), 15 May 1979, pp. 627-629.

16. Hartley, N. E. W., "Ion Implantation and Surface Modification in Tribology", Wear, 34(1975), pp. 427-438.

17. Longworth, G. and N. E. W. Hartley, "Mossbauer Effects Study of Nitrogen-Implanted Foils", Thin Solid Films, 48(1978), pp. 95-104.

18. Dearnaley, G., "Applications of Ion Implantation in Metals", Thin Solid Films, V. 107, 1913, pp. 315-326.

19. Butler, J. W., loc. cit., p. 9.

20. Wilbur, Paul, J. and Larry O. Daniels, Broad Beam Ion Implantation Research, presented at IPAT Conference in Munich, West Germany, May 1985.

21. Blamires, N. G., "The Influence of Ion Beam Current Densities on the Electrical Properties of Boron Implanted Silicon", In Ion Implantation in Semiconductors, eds. I. Ruge and J.Graul, Springer-Verlag, Berlin, West Germany, 1971, pp. 119-123.

22. Harris, J. S., "The Effects of Dose Rate and Implantation Temperature on Lattice Damage and Electrical Activiy in Ion-Implanted GaAs", In Ion Implantation in Semiconductors, eds. I. Ruge and J. Graul, Springer-Verlag, Berlin, West Germany, 1971, pp. 157-167.

23. Merz, J. L., et. al., "Implantation of Bi into GaPIII. Hot-Implant Behavior", In Ion Implantation in Semiconductors, eds. I. Ruge and J. Graul, Springer-Verlag, Berlin, West Germany, 1971, pp. 182-192.

REFERENCES (cont'd)

24. Meek, R. L., W. M. Gibson, and J. P. F. Sellschop, "Dimpling-a New Manifestation of Ion Produced Lattice Damage", In Ion Implantation in Semiconductors, eds. I. Ruge and J. Graul, Springer-Verlag, 1971, Berlin, West Germany, pp. 297-298.

25. Wilson, Robert G. and George R. Brewer, Ion Beams with Applications to Ion Implantation, John Wiley and Sons, New York, 1973, pp. 310, 311.

26. Sze, S. M., Physics of Semiconductor Devices, 2nd edition, John Wiley and Sons, New York, 1981, p. 70.

27. Ross, Robert B., Metallic Material, Chapman and Hill Ltd., London, England, 1968, pp. 626, 629, 693.

TA 459
R65

28. Brewer, George R., Ion Propulsion, Gordon and Breach Science Publishers, New York, 1970, pp. 127-8.

29. Wilbur, Paul J. and Larry O. Daniels, "Broad Beam Ion Implantation Research", to be published in Vacuum.

30. Davis, L. E., ed., Handbook of Auger Electron Spectroscopy, 2nd edition, Physical Electronics Industries, Eden Prairie, Mn., 1976, p. 13.

31. Prutton, M., Surface Physics, Oxford University Press, London, England 1975, p. 15.

32. Townsend, P. D., loc. cit., pp. 25-30.

33. Clark, Donald S. and Wilbur R. Varney, Physical Metallurgy for Engineers, D. Von Nostrand Company, Inc., 3rd printing, New York, 1955, p. 210.

34. Feller, H. G., R. Klinger, and W. Benecke, "Tribo-Enhanced Diffusion of Nitrogen Implanted Steels", Materials Science and Engineering, 69(1985), pp. 173-180.

35. Bone, W. M., et. al., "Summary Abstract: Sims, Auger, and Nuclear Reaction Analysis of N-implanted Fe Alloys", J. Vac. Sci. Technol., A2(2), April-June 1980, pp. 788-789.

36. Whitton, J. L., et. al., "Chrominum Nitride and Martensite Formation in Nitrogen-implanted Single-Crystal Stainless Steel", Materials Science and Engineering, 69(1985), pp. 111-116.

REFERENCES (cont'd)

37. Singer, I. L. and J. S. Murday, "Chemical State of Ion-Implanted Nitrogen in Fe18Cr8Ni Steel", J. Vac. Sci. Technol., 17(1), Jan.-Feb. 1980, pp. 327-329.

38. Hutchings, R., "The Subsurface Microstructure of Nitrogen-Implanted Metals", Materials Science and Engineering, 69(1985), pp. 129-138.

39. Meyers, S. M., D. E. Amos, and D. K. Brice, "Modeling of Enhanced Diffusion under Ion Irradiation", J. Appl. Phys., Vol. 47, No. 5, May 1976, pp.1812-1819.

40. Rehn, L. E., R. S. Averback, and P. R. Okamoto, "Fundamental Aspects of Ion Beam Surface Modification: Defect Production and Migration Processes", Materials Science and Engineering, 69(1985), pp.1-11.

41. Adda, Y., M. Beyeler, and G. Brebec, "Radiation Effects on Solid State Diffusion", Thin Solid Films, 25(1975), pp. 107-156.

APPENDIX A

Temperature Profiles of AISI Type-304 Stainless Steel Block Surfaces during Nitrogen Ion Implantation

The surface temperature of AISI type-304 stainless steel blocks was recorded during nitrogen ion implantation. The blocks were mounted in a water-cooled copper fixture with iron-constantan thermocouples mounted in the bottom of a hole drilled from the downstream side of the blocks to within 0.1 mm from the implanted block surfaces. The nitrogen ion beam was directed at normal incidence toward the blocks for a period of time and then shut off. Figures A.1, A.2 and A.3 show the block surface temperatures as a function of time at various ion beam current densities.

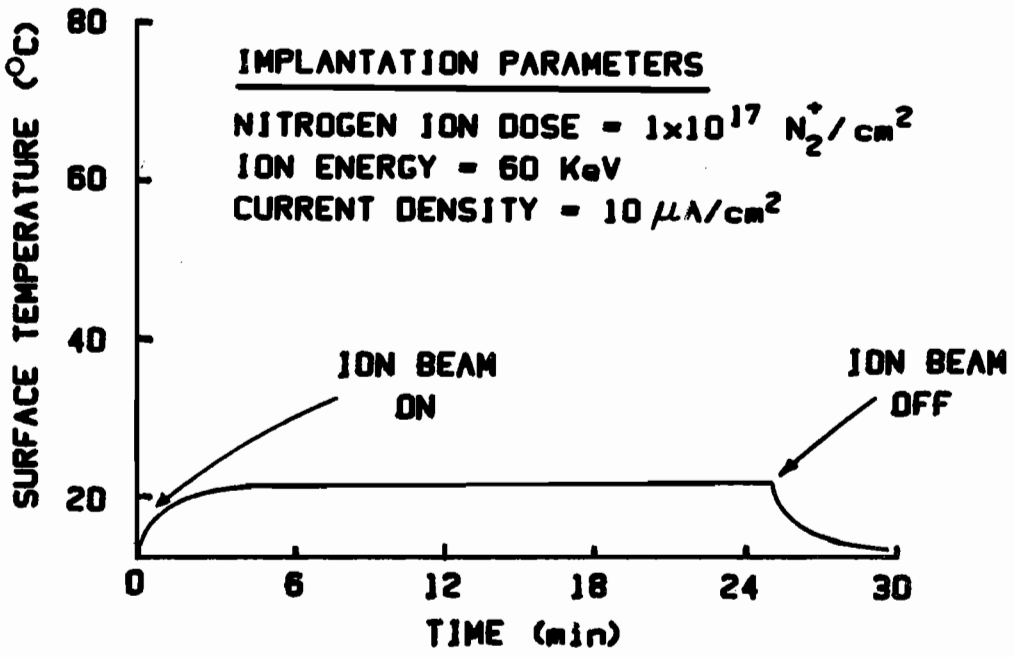

Figure A.1. Surface Temperature of an AISI Type-304 Stainless Steel Block during Implantation at an Ion Beam Current Density of 10 $\mu A/cm^2$

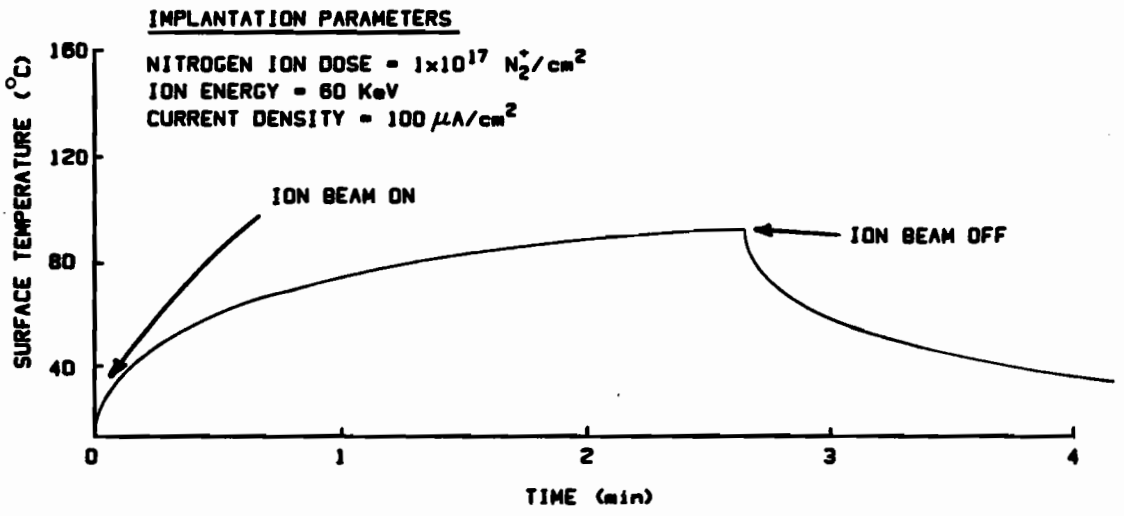

Figure A.2. Surface Temperature of an AISI Type-304 Stainless Steel Block during Implantation at an Ion Beam Current Density of 100 $\mu A/cm^2$

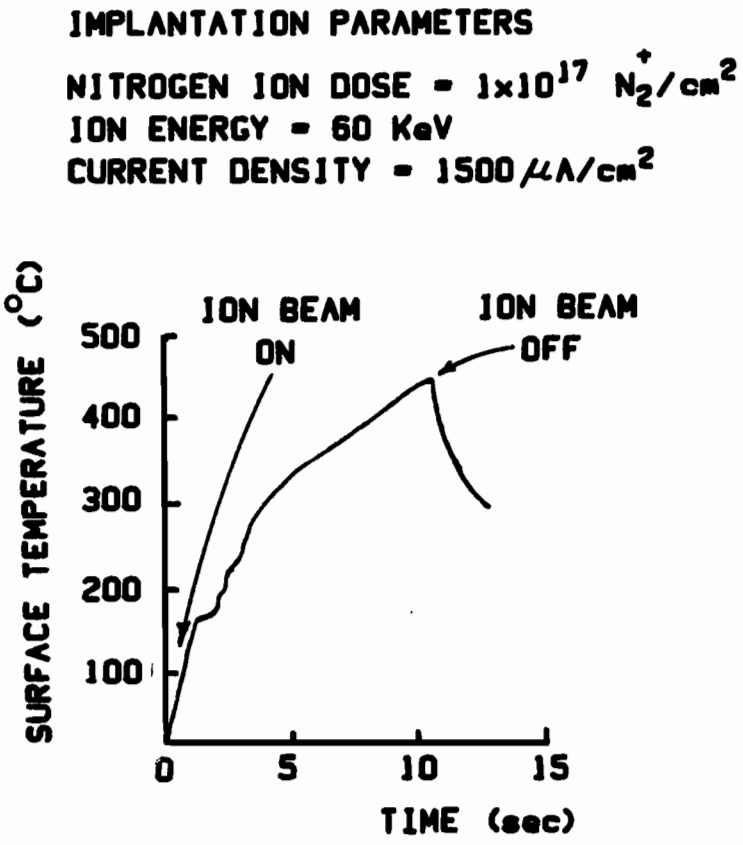

Figure A.3. Surface Temperature of an AISI Type-304 Stainless Steel Block during Implantation at an Ion Beam Current Density of 1500 $\mu A/cm^2$

APPENDIX B

Sputtering Rate Determination of Various Steels

The rate K(cm/min), at which material is removed from a steel surface due to argon ion bombardment is given by the following equation:

$$K = \frac{d_N}{\int_1^{tf} n\,dt - (tf - 1)n_{tf}} \qquad \text{(B-1)}$$

where d_N(atoms/cm^2) is equal to the dose of nitrogen atoms per unit area implanted through a steel surface, n(atoms/cm^3) is the atom density of nitrogen in the surface, t(min) is the sputtering time, tf(min) is the longest time at which n was found for a particular sample and n_{tf}(atoms/cm^3) is the baseline nitrogen atom density corresponding to the longest sputtering time for a particular sample analysis. Figure B.1 shows a typical plot obtained directly from Auger spectroscopic data of nitrogen atom density as a function of sputtering time. The cross-hatched area under the curve represents the denominator portion of Eq. B-1. Because the nitrogen atom density at the maximum sputtering time frequently was not zero (as shown in the figure), only the area under the curve to the baseline nitrogen atom density was used. This was only a minor correction because the baseline density was less than 5% of the maximum nitrogen atom density for all the Auger spectroscopic data.

Using Eq. B-1, the sputter rate was found to vary from about 1.7 nm/min to 3.3 nm/min for AISI type-304 stainless steel. The nitrogen

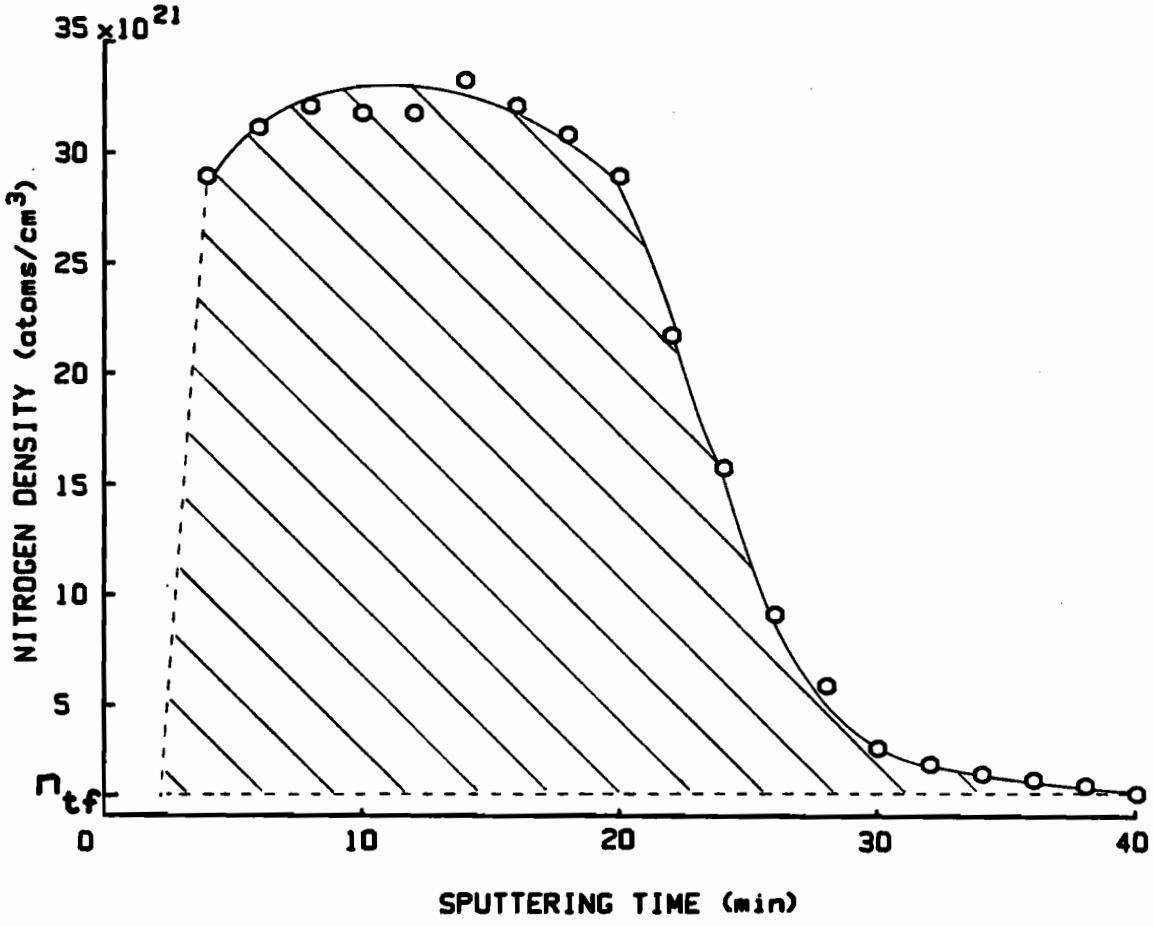

Figure B.1. Typical Plot Used to Find the Sputter Rate of Steels Using an Argon Ion Gun.

dose in each sample did not seem to affect the way that the sputter rate varied. Therefore, the average values for K were used for each type of steel. These values along with their standard deviations are shown in Table B.1.

Table B.1

Argon Ion Sputter Rates of Various Steels

Steel	K (nm/min)	Standard Deviation (nm/min)	Number of samples K was obtained from
AISI M2 tool steel	5.0	0.5	3
SAE O1 tool steel	5.5	1.0	2
AISI type-304 stainless steel	2.5	0.5	14

APPENDIX C

Actual Nitrogen and Carbon Concentration Analysis

Because the raw Auger spectroscopic data were obtained assuming nitrogen, iron and sometimes carbon were the only species contained in the steel samples, analysis had to be accomplished to account for the presence of other constituents (e.g., chromium, nickel, tungsten, molybdenum, vanadium and magnesium). The data that were obtained from Auger analysis represent the following parameters:

$$C_N^* = \frac{N_N}{N_N + N_{Fe} + N_C} \qquad \text{(C-1)}$$

$$C_C^* = \frac{N_C}{N_N + N_{Fe} + N_C} \qquad \text{(C-2)}$$

$$C_{Fe}^* = \frac{N_{Fe}}{N_N + N_{Fe} + N_C} \qquad \text{(C-3)}$$

where C_N^*, C_C^* and C_{Fe}^* represent known Auger nitrogen, carbon and iron concentrations, respectively in the implanted near-surface layers if only nitrogen, carbon and iron were present in the samples, and N_z represents the number of atoms of species z in the same region. The actual nitrogen and carbon concentrations C_N(atom%) and C_C(atom%), respectively for AISI type-304 stainless steel are represented by the following equations:

$$C_N = \frac{N_N}{N_N + N_{Fe} + N_{Ni} + N_C} \qquad (C-4)$$

$$C_C = \frac{N_C}{N_N + N_{Fe} + N_{Ni} + N_C} \qquad (C-5)$$

Equations C-4 and C-5 can be written in the following forms:

$$C_N = \frac{1}{1 + \frac{N_{Fe}}{N_N} + \frac{N_{Fe}}{N_N}\left[\frac{N_{Cr}}{N_{Fe}} + \frac{N_{Ni}}{N_{Fe}} + \frac{N_C}{N_{Fe}}\right]} \qquad (C-6)$$

$$C_C = \frac{1}{1 + \frac{N_{Fe}}{N_C} + \frac{N_{Fe}}{N_C}\left[\frac{N_{Cr}}{N_{Fe}} + \frac{N_{Ni}}{N_{Fe}} + \frac{N_C}{N_{Fe}}\right]} \qquad (C-7)$$

To find the actual nitrogen and carbon concentrations from Equations C-6 and C-7, the ratios N_{Fe}/N_N, N_{Cr}/N_{Fe}, N_{Ni}/N_{Fe} and N_C/N_{Fe} are required. This is accomplished by using the following equations for the known pre-implantation chromium (C'_{Cr}), nickel (C'_{Ni}) carbon (C'_C) and iron (C'_{Fe}) concentrations i.e.,

$$C'_{Cr} = \frac{N_{Cr}}{N_{Fe} + N_{Cr} + N_{Ni} + N_C} \qquad (C-8)$$

$$C'_{Ni} = \frac{N_{Ni}}{N_{Fe} + N_{Cr} + N_{Ni} + N_C} \qquad (C-9)$$

$$C'_C = \frac{N_C}{N_{Fe} + N_{Cr} + N_{Ni} + N_C} \qquad (C-10)$$

$$C'_{Fe} = \frac{N_{Fe}}{N_{Fe} + N_{Cr} + N_{Ni} + N_C} \qquad \text{(C-11)}$$

The combinations of Equations C-1, C-2, C-3, C-6, C-7, C-8, C-9, C-10 and C-11 results in the following equations for the actual nitrogen and carbon concentrations in nitrogen-implanted AISI type-304 stainless steel samples:

$$C_N = \frac{1}{\frac{1}{C^*_N} + \frac{(1 - C^*_N - C^*_C)}{C^*_N C'_{Fe}}(C'_{Cr} + C'_{Ni} + C'_C)} \qquad \text{(C-12)}$$

$$C_C = \frac{1}{\frac{1}{C^*_C} + \frac{(1 - C^*_N - C^*_C)}{C^*_C C'_{Fe}}(C'_{Cr} + C'_{Ni} + C'_C)} \qquad \text{(C-13)}$$

The equations for the actual nitrogen and carbon concentrations in the tool steels are the same as Equations C-12 and C-13, except the concentrations of the constituents in the tool steels are substituted for the atom concentrations appearing in the parenthesis in Equations C-12 and C-13.

This analysis was accomplished assuming that the concentrations of the constituents did not change relative to each other due to ion implantation (i.e., chromium did not diffuse preferentially over nickel from the implanted region).

APPENDIX D

Block Wear Volume Determination

The volume of material removed from a block is found by finding the area of the cross-hatched region shown in Fig. D.1 and multiplying it by the block width. In the figure, L(mm) is the wear scar length, r_R(mm) is the radius of a ring and θ(radians) is the subtended angle associated with L. The block is drawn in the figure in such a way that the ring that had worn against the block, rotated against the lower part of it in the clockwise or counterclockwise θ-direction. To find the cross-hatched area, the triangular area (area from point P to the block surface) is subtracted from the "pie-shaped" area (area including triangular and cross-hatched regions). The "pie-shaped" area A_p(mm^2), is found from the following equation:

$$A_P = \frac{\theta}{2} r_R^2 \qquad \text{(D-1)}$$

where θ(rad) is given by Eq. D-2.

$$\theta = 2 \sin^{-1} \frac{L}{2r_R} \qquad \text{(D-2)}$$

The triangular area A_T(mm^2) is found from the following equation:

$$A_T = \frac{L}{2}\left(r_R^2 - \frac{L^2}{4}\right)^{\frac{1}{2}} \qquad \text{(D-3)}$$

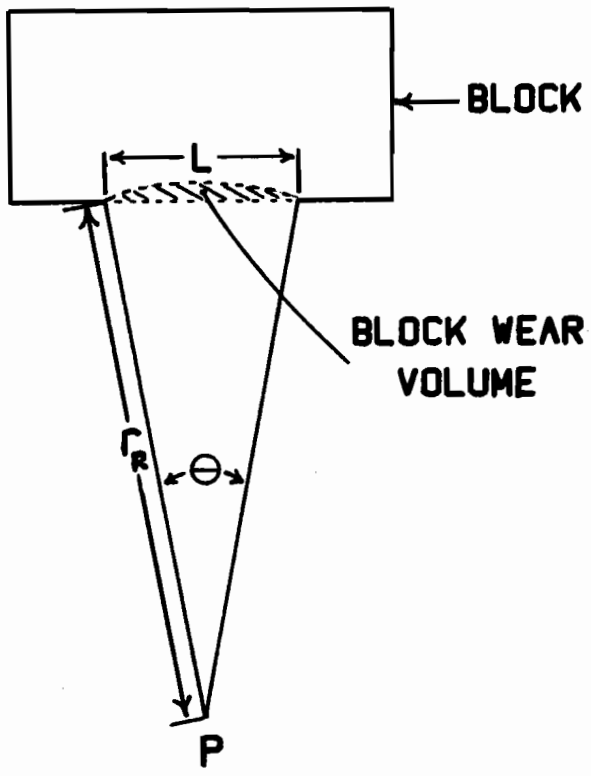

Figure D.1. Schematic for Block Wear Volume Determination

Combining Equations D-1 and D-2, subtracting Eq. D-3 from this and multiplying by the block width W(mm), results in Eq. D-4 to determine the block wear volume, $V(mm^3)$.

$$V = \left[r_R^2 \sin^{-1} \frac{L}{2r_R} - \frac{L}{2}\left(r_R^2 - \frac{L^2}{4}\right)^{1/2} \right] W \qquad \text{(D-4)}$$

APPENDIX E

Range Calculation

The projected range, $R_p(\mu g/cm^2)$ (average distance that an ion travels inward perpendicular to a target surface) of nitrogen ions in iron is found with the following equation from Ref. 32:

$$R_P \simeq C_1\left(\frac{M_2}{M_1}\right) M_2 \frac{(Z_1^{\frac{2}{3}} + Z_2^{\frac{2}{3}})^{\frac{1}{2}} E}{Z_1 Z_2} \qquad \text{(E-1)}$$

where $C_1(M_2/M_1)$ is a factor which varies with the ratio of atomic weights as shown in Fig. E.1, M_2 is the atomic weight of implantation target atoms, Z_1 is the atomic number of an implanted ion, Z_2 is the atomic number of target atoms and E (keV) is ion energy. It should also be noted that M_1 is the atomic weight of an implanted ion. Knowing that $M_2/M_1 = 2$ for iron and molecular nitrogen (most of the ion beam in this study was composed of N_2^+), the factor $C_1(M_2/M_1)$ is found from Fig. E.1 to be about 0.69. Upon substitution of the ion energy, the appropriate atomic weights and atomic numbers , $C_1(M_2/M_1)$ into Eq. E-1 and dividing the resultant by the density of iron, the projected range is found. For 60 keV nitrogen into pure iron, the calculated range is ~55 nm.

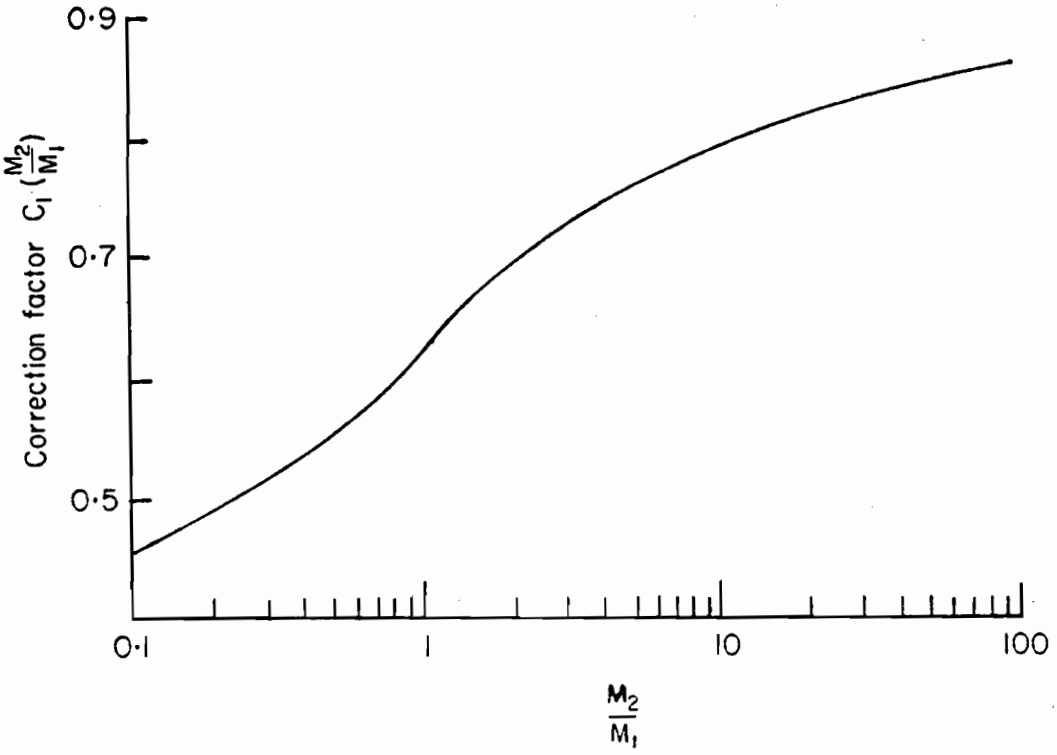

Figure E.1. The Correction Factor for Equation E-1 Used by Schiott (1970) for Intermediate Energy Ions (from Townsend et al)